Science of the Total Environment 1022 (2026) 181622

Contents lists available at ScienceDirect

Science of the Total Environment

journal homepage: www.elsevier.com/locate/scitotenv

Hybrid particulate matter generated by lava-ignited wildfires at the Litli-Hrútur 2023 eruption, Iceland

Laura Wainman [a,*], Evgenia Ilyinskaya [a], Melissa Anne Pfeffer [b], Penny E. Wieser [c], David Damby [d], James B. McQuaid [a], Celine Mandon [b], Enikö Bali [e], Josefa Sepulveda-Araya [a], Richard Walshaw [f], Caleb Hall [f], Stuart Micklethwaite [f], Zabeada Aslam [f], Samantha J. Hammond [g], Barbara Kunz [g], Frances Jenner [g], Andri Stefánsson [c], Sæmundur A. Halldórsson [c], Jóhann Gunnarsson Robin [c], Alessandro Aiuppa [h], Tamsin A. Mather [i]

[a] School of Earth and Environment, University of Leeds, Leeds, UK
[b] Icelandic Meteorological Office, Reykjavík, Iceland
[c] Earth and Planetary Science, UC Berkeley, Berkeley, USA
[d] U.S. Geological Survey (USGS), Volcano Science Center, Moffett Park, CA, USA
[e] Institute of Earth Sciences, University of Iceland, Reykjavik, Iceland
[f] Leeds Electron Microscopy and Spectroscopy Centre (LEMAS), Bragg Centre for Materials Research, University of Leeds, UK
[g] School of Environment, Earth and Ecosystem Sciences, Open University, Milton Keynes, UK
[h] Dipartimento di Scienze della Terra e del Mare, Università degli Studi di Palermo, Palermo, Italy
[i] Department of Earth Sciences, University of Oxford, Oxford, UK

HIGHLIGHTS

- Lava flows at the 2023 Litli-Hrútur eruption in Iceland ignited extensive moss wildfires.
- We collected samples of endmember and mixed volcanic and wildfire emissions, including gas and particulate matter (PM).
- Mixing between emissions resulted in agglomeration and scavenging of volcanic aerosols by wildfire PM to form hybrid PM.
- Hybrid PM had altered physicochemical charactersitics relative to end-member volcanic and wildfire emissions.
- Modified physicochemical characteristics could result in new pathways for toxic metals and gaseous pollutants.

GRAPHICAL ABSTRACT

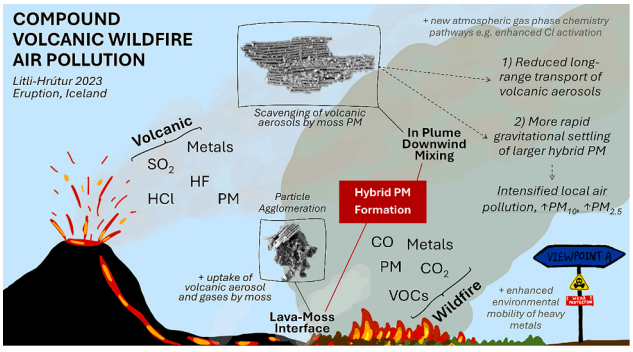

ARTICLE INFO

Keywords:
Volcanic eruption
Wildfire

ABSTRACT

Lava flows from the Litli-Hrútur 2023 eruption ignited the largest moss wildfires since modern record keeping in Iceland began. Volcanically ignited wildfires present a cascading and more complex hazard than standalone volcanic eruptions and are likely to become more frequent globally due to climate change. Both volcanic

* Corresponding author.
E-mail address: eelrw@leeds.ac.uk (L. Wainman).

https://doi.org/10.1016/j.scitotenv.2026.181622
Received 17 December 2025; Received in revised form 2 February 2026; Accepted 25 February 2026

Air pollution
Particulate matter
Compound event

eruptions and wildfire events generate well-characterized air pollution hazards through the emission of gas and particulate matter, but the physicochemical consequences of mixing between end-member emission types during compound events remain poorly understood. In this study, we collected samples of end-member volcanic, wildfire, and mixed plume particulate matter during the Litli-Hrútur 2023 eruption and wildfires. Geochemical and morphological analysis showed that wildfire smoke and lava flow outgassing have distinctive chemical signatures and particulate matter (PM) size distributions, but that when mixing occurs between them, either directly at the lava-moss burning interface or during downwind transport, it can result in the formation of hybrid PM. This hybrid PM may be formed through mechanical interactions via well-established processes such as agglomeration and particle scavenging, although these interactions are unique in the context of a compound volcanic-wildfire event as they occur between emissions from two different sources. We demonstrate that the formation of hybrid PM via these mechanisms may result in altered physicochemical characteristics, and suggest that this may have consequences for depositional processes and atmospheric and environmental transport pathways of key species when compared to stand-alone volcanic eruptions.

1. Introduction

The likelihood of compound volcanic-wildfire events is increasing globally due to continued planetary warming and changes in global weather patterns (Mansoor et al., 2022). Compound volcanic-wildfire events can occur when an eruption happens coincidentally to an existing wildfire or, depending on the style of eruption, a wildfire may be ignited by volcanic products, such as lava flows, incandescent ballistics, or pyroclastic flows (Yong Quah et al., 2023). Extended periods of hot and dry weather due to climate change mean that some of the environments (e.g., forests, peatbog, grassland, and steppe) surrounding active volcanoes are becoming more vulnerable to ignition by all causes, including volcanically triggered events (Fink and Ajibade, 2022). Although on a regional scale, the forecast of wildfire modification due to global changes can be ambiguous, for example in Iceland where an increase in frequency of extreme weather includes both heavy precipitation and extended dry periods (Icelandic Meteorological Office, 2018), impacting both vegetation production and fuel load. Several volcanically ignited wildfires have been documented to date during flank eruptions at Kīlauea (Hawai'i) between 1983 and 2018 (Meredith et al., 2022), at Pacaya Volcano (Guatemala) in 2010 (Wardman et al., 2012), at the eruption of Stromboli (Italy) in 2019 (Turchi et al., 2020; Iacono et al., 2025), at the Tajogaite eruption on La Palma in 2021 (Shatto et al., 2024), and most recently at the eruptions in Iceland on the Reykjanes Peninsula between 2021 and 2025 (Schiffmann et al., 2025). It is likely that other volcanic-wildfire events have also occurred across the globe but are undocumented in the scientific literature.

One of the primary hazards associated with compound volcanic-wildfire events is the simultaneous emission of wildfire smoke and volcanic aerosols, both of which can individually worsen air quality on a regional scale (Volcanic eruptions: Kajino et al., 2004, Schmidt et al., 2015, Whitty et al., 2025; Wildfires: Selimovic et al., 2019, Adachi et al., 2022, Holder et al., 2023). Wildfire emissions contain reactive gases (CO, CO_2, CH_4, volatile organic compounds – VOCs, and nitrogen oxides - NO_X) and particulate matter (PM), including black and brown carbon (Selimovic et al., 2019; Holder et al., 2023; Wilson et al., 2025), whilst volcanic eruptions can emit significant quantities of silicate ash, gases (including H_2O, CO_2, SO_2, HCl, HF), PM and trace metal species (Nriagu, 1989; Delmelle, 2003; Mather et al., 2003; Aiuppa, 2009). The end-member compositions of these emissions have been well constrained individually; however, to date very few studies have investigated the processes that occur during compound events when volcanic and wildfire emissions mix in the atmosphere. Atmospheric mixing and the co-presence of volcanic and wildfire emissions is likely to result in mechanical interactions and chemical reactions and thus potentially facilitate the formation of hybrid PM. In this study, we consider hybrid PM to be that which has altered physical or chemical properties as a consequence of mechanical interactions and/or chemical reactions that occur upon mixing between emissions from difference sources. Such physicochemical alterations could include, but are not limited to, changes in bulk PM size distribution (e.g., via scavenging or agglomeration effects), as well as alterations to element water solubility or changes in element speciation behaviour. Such changes could have consequences for the environmental reactivity and mobility of key pollutant species, as well as their bioavailability. Given that exposure to volcanic and wildfire emissions separately has been linked to negative health effects in humans (including an increased prevalence of respiratory and cardiovascular disease, as well as higher rates of overall morbidity and mortality (Reid et al., 2016, Stewart et al., 2021), understanding and mitigating human exposure to hybrid volcanic-wildfire emissions is of critical importance for protecting population health during compound volcanic-wildfire events. Furthermore, extreme environmental change in Earth's deep past associated with extended episodes of volcanism have in some cases shown evidence of increased wildfire occurrence emphasising the importance of understanding the environmental consequences of these interactions on a planetary scale (e.g., Chu et al., 2020).

In this study, we investigate the air quality impacts of a compound volcanic-wildfire event at the Litli-Hrútur 2023 eruption and lava-ignited wildfires on the Reykjanes Peninsula in Iceland. We examine the atmospheric processes that occurred during the simultaneous emission of gases and PM from the volcanic vent, lava flows, and wildfire vegetation burning. We focus on the formation of hybrid PM as a result of mechanical interactions between volcanic and wildfire particles and gaseous species in the mixed plume and suggest that this hybrid PM may have distinct physicochemical characteristics compared to end-member volcanic and wildfire emissions. We propose that this may alter the atmospheric transport and environmental dispersion pathways of key elements, with possible implications for regional air quality and human exposure to harmful pollutant species. Given the increasing likelihood of future volcanically ignited wildfire events globally, future volcanic hazard mitigation planning could integrate the unique air quality threat posed by compound-volcanic wildfire events.

1.1. The Litli-Hrútur 2023 eruption and wildfires

The effusive Litli-Hrútur eruption began on 10th July 2023 and lasted three and a half weeks before ceasing on 5th August 2023. The eruption occurred to the northeast of the previous Geldingadalir (2021) and Meradalir (2022) eruptions (Fig. 1d). The eruption generated a total lava volume of approximately 15.9 million m^3 covering an area of ~1.5 km^2. The eruption began with multiple effusive fissures stretching over 1 km in length, before ultimately focusing into a single crater. The lava composition was similar to the end of the previous eruption in 2022 suggesting it derived from a similar magmatic source at depth (Caracciolo et al., 2025).

The occurrence of the eruption in July–August 2023 coincided with an extended period of hot and dry weather in Iceland (Veðurstofa íslands, 2023). Climate-related forecasts over the next few decades for Iceland suggest more frequent extreme weather, including both heavy rainfall and dry spell periods. The extended dry period in June 2023 may, therefore, have contributed to the occurrence of extensive wildfires

during the July 2023 eruption, compared to only very minor wildfires during the previous eruptions in 2021 and 2022 (Schiffmann et al., 2025). The vegetation surrounding the eruption site, which includes grasses, dwarf-shrubs, herbs and mosses, was potentially drier as a result and thus readily ignited by advancing lava flows when the eruption occurred (Fig. 1b). Once ignited, smouldering spread rapidly through the moss with some areas of open flame burning. This resulted in a total burn area of ~2.5 km^2, with the smoulder front being up to 1 km from the active lava flows in some cases, and making it the largest moss wildfire since modern record keeping in Iceland began in 2006 (Fig. 1c and d and Fig. 2;, Icelandic Institute of Natural History, 2023, Schiffmann et al., 2025).

Wildfire burning generated dense clouds of smoke which impeded both visibility and ground level air quality over an extensive area around the eruption site (Fig. 1c). Outgassing lava flows contributed additional, but more localised, ground level air pollution, although emissions from the main volcanic vent were generally buoyant and thus were concentrated at higher altitudes with only periodic grounding. Access to the Viewpoint E (Fig. 2a), which was the favoured hiking route by tourists at the beginning of the eruption, required a ~ 8–10-hr round trip hike through areas which were regularly inundated with smoke from wildfire burning and were within proximity of nearby outgassing lava flows. Hiking Trail A was more removed from the immediate moss burning, partly due to topography, but Viewpoint A, being closer to the volcanic vent and burning moss scarp was regularly inundated with both volcanic emissions and wildfire smoke. The risk of combined exposure to air pollution from both volcanic degassing and dense wildfire smoke raised concerns about potential health impacts on tourists visiting the eruption site by civil protection agencies and resulted in the temporary closure of the eruption site to tourists (Almannavarnir, 2023). In this study, we present the results from an emergency response air quality monitoring campaign, led by the Icelandic Meteorological Office on 16th July 2023, during the closure of the eruption site and shortly after the onset of the eruption.

2. Methods

2.1. Sampling approaches

2.1.1. Filter packs

Filter packs mounted on (i) UAV (uncrewed aerial vehicle, DJI Matrice 300 RTK, Wainman, 2024) and (ii) ground-level apparatus were used to collect in-situ samples of gases and aerosol PM from volcanic and wildfire emissions, respectively. Sampling altitude with the UAV ranged between 50 and 80 m above the flight take off point. Where multiple flights were used to collect one sample the pump was turned off whilst the UAV was grounded to minimize the uptake of ground-based dust. The UAV sampling set up consisted of a 4-stage Teflon (Dupont) filter pack holder secured to the UAV "leg", connected via PVC tubing to a pump (SKC Leland Legacy) mounted on the body of the UAV (Fig. 2b). The combined weight of the filter pack and pump (and on-board multiGAS; see Section 2.1.3) was just under the payload capacity of the UAV (Max payload: 2.7 kg). Care had to be taken to ensure a balanced weight distribution on the UAV to avoid issues upon take-off and landing. The ground-level filter pack sample (LHFP5) was collected along Hiking Trail E, used by tourists to reach Viewpoint E (Fig. 2c). This was done using a portable backpack frame with the same filter pack and pump set up as used for the UAV sampling. Further details on the filter holder configuration and filter preparation via base treatment prior to sampling are provided in the supplementary document. Note throughout the sampling process all team members wore half-face respirators with combined gas, vapor, and particulate cartridges (e.g. 3 M 6000 Series).

ˆSimultaneous on-board MultiGAS during sample collection. For the samples with on-board MultiGAS SO2 timeseries was used to correct the total volume pumped for the time spent in the plume. Where on-board MultiGAS was not available the total volume pumped was used instead.

2.1.2. Cascade Impactors

The use of cascade impactors is similar to that of filter packs, where the impactor is connected to an air pump which draws air through a series of stages containing PTFE filters for sampling. SKC Sioutas cascade impactors consist of four stages plus an after stage and can thus resolve particles into a series of five size bins of decreasing particle diameter ranges from stage A (> 2.5 μm), B (2.5 μm – 1 μm), C (1 μm – 0.5 μm), D (0.5 μm – 0.25 μm), to the final after stage E (< 0.25 μm). A cascade impactor was used to collect a size-resolved PM sample at ground level along the tourist Hiking Trail E (Fig. 2a). This cascade impactor sample (LHSKC2) was collected simultaneously to filter pack sample LHFP5. See supplementary datasheet S3 for cascade impactor trace element data.

2.1.3. MultiGAS

A multi-GAS instrument from University of Palermo (Aiuppa, 2005; Liu et al., 2020) was installed on the UAV for time-series measurements of major gas concentrations (time resolution 1 Hz). This aerial multiGAS, used previously during eruptions in Iceland (Halldórsson et al., 2022), contains SO_2 and H_2S electrochemical sensors (City Technology; T3ST/F-TD2G-1 A and T3H-TC4E-1 A, calibrated for 0 to 200 ppmv and 0 to 50 ppmv respectively, see Liu et al., 2020), and an infrared spectrometer for CO_2 (Microsensorik Smartgas Modul Premium2, range 0 to 5000 ppmv).

Time-averaged in-plume SO_2 concentrations for filter pack and impactor samples were calculated using the multi-GAS SO_2 timeseries

Table 1
Filter Pack and Cascade Impactor Sample Overview and Metadata.

Sample ID	Sample Type	Sample Location	Sampling Date	Filter Set Up	Flow Rate (L/min)	Sample Duration (mins)	Volume Pumped (L)	Mass % Filter for SEM Analysis***
LHFP1	Filter Pack	UAV Lava-Moss Contact	13/07/2023	PM + 3G*	10.1	1**	10.2	7
LHFP2	Filter Pack	UAV Above Lava Flow	13/07/2023	PM + 3G	9	43.5	312.1	13.5
LHFP5	Filter Pack	Ground-level Hiking Trail E	16/07/2023	PM Only	9	35	315.1	8
LHFP8	Filter Pack	UAV At-Vent	19/07/2023	PM Only + MGˆ	9	61	549.6	0
LHSKC1	Impactor	UAV Lava-Moss Contact	13/07/2023	PM Only (5 Stages)	9	12.2	109	0
LHSKC2	Impactor	Ground-level Hiking Path	16/07/2023	PM Only (5 Stages)	9	35	315.1	0
LHSKC3	Impactor	UAV At-Vent	16/07/2023	PM Only (5 Stages) + MGˆ	9	30	270.3	0

* PM + 3G refers to the filter set up containing one PTFE PM filter +3 base-treated gas filters on the subsequent stages.
** The limited sampling duration reflects a technical issue with the pump set up where the tubing became twisted and thus cut off the flow of the pump.
*** The % (by mass) of each filter cut out for SEM analysis is included and was corrected for when processing of the ICP-MS results.

where sample collection had on-board multiGAS, excluding data <0.5 ppmv (the baseline between in-plume peaks in SO_2) within the known flight-time window. The time-averaged SO_2 concentrations should be viewed as minimum values as some in-plume measurements were made when SO_2 concentrations were above the maximum detection limit of the sensor (saturation occurred at ~220 ppmv, note post-saturation measurements are also associated with higher uncertainty whilst the sensor returns to a reliable response following saturation). The total time filter pack and impactor samples spent inside the aerosol plume (defined as $SO_2 > 0.5$ ppmv) was used to correct the total volume pumped for the in-plume volume sampled where possible. See supplementary datasheet S4 for raw MultiGAS measurements.

2.1.4. Optical particle spectrophotometer

As part of the emergency air quality monitoring campaign on 16th July an optical particle spectrophotometer (OPS; TSI 3330) was deployed at several locations around the eruption site to rapidly assess ground-level airborne concentrations of PM_{10} and $PM_{2.5}$. The OPS used is a reference grade instrument which measures number concentrations of particles between 0.3 and 10 μm across 16 size bins, with a maximum particle count of 3000 particle cm^{-3} (Vasilatou et al., 2021). OPS measurement locations around the Litli-Hrútur eruption site are shown on Fig. 2a and measurement details are included in Table 2, with photographs of the deployed OPS included in Supplementary Figs. S1 and S2. The OPS was used at ground level and was considered representative of the potential exposure for tourists hiking along the path to reach the eruption viewpoint.

Concentrations of $PM_{2.5}$ and PM_{10} were calculated by manually reprocessing the raw particle count data, downloaded from the OPS instrument, and following a series of assumptions. The standard approximation of spherical particles of uniform density was applied. We also chose to calculate a volume weighted diameter (D_{pv}) for each size bin, rather than a geometric diameter, for consistency with the OPS software (AIM Software) and Crilley et al. (2018). Bin cutoffs are lower size bounds (Bin 1: 0.3–0.374 μm, Bin 17: > 10 μm). Particle count concentrations were then converted to particle mass measurements following Eq. 1 – Eq. 3. in Crilley et al. (2018). Changes in the assumed particle density can result in significant variations in the particle mass measurement outputs so we therefore perform our conversion with an average density of 1.7 g/cm^3, a maximum density of 2.3 g/cm^3 (volcanic

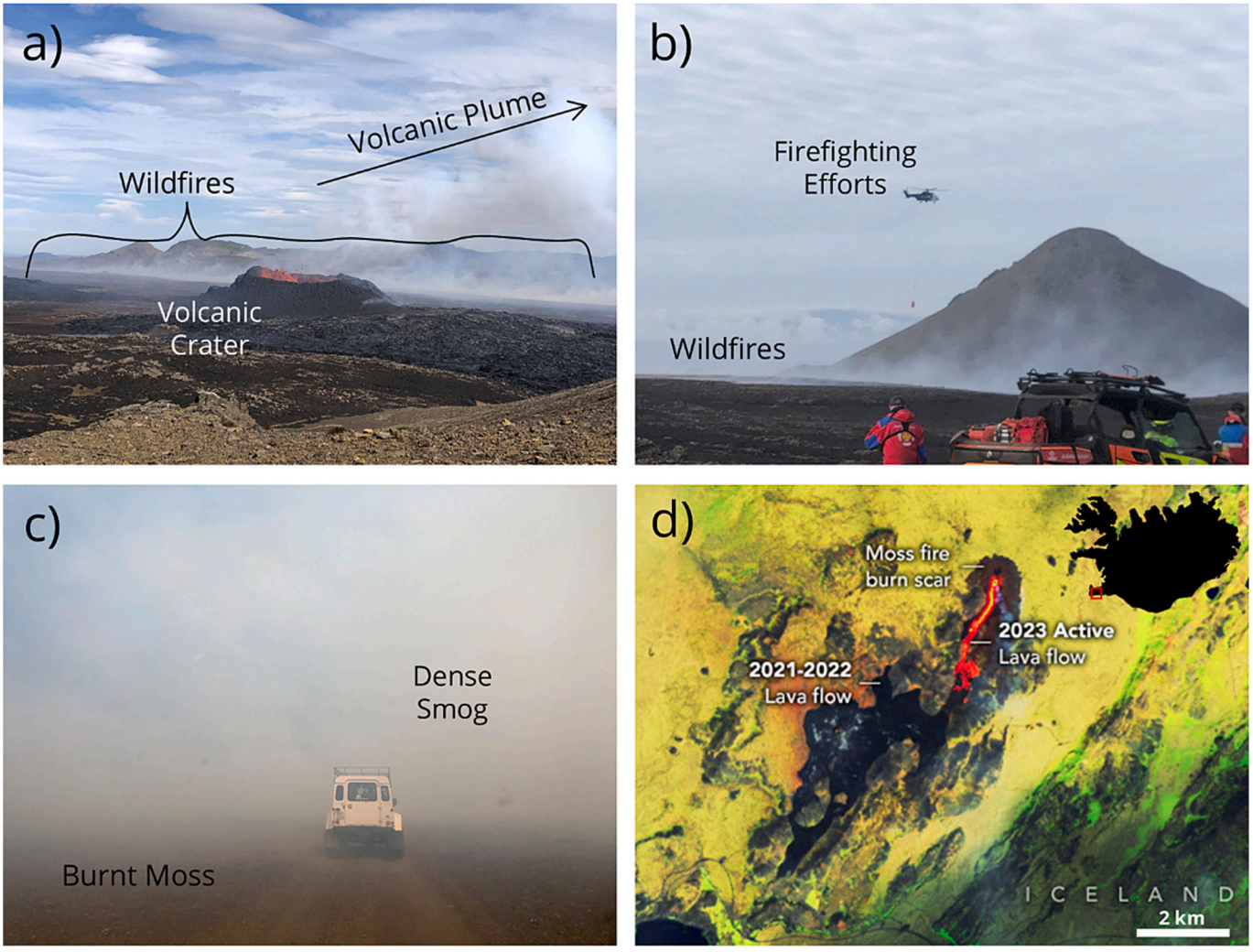

Fig. 1. The Litli-Hrútur 2023 Eruption and Lava-Ignited Wildfires. a) Photograph of the Litli-Hrútur eruption crater. Fire fountaining is visible over the volcanic crater rim. The volcanic plume can be seen as degassing occurs from the vent, is advected upwards due to buoyancy, and is dispersed down wind. Wildfire smoke can be seen in the background at the edge of the lava field where it ignited the moss which covers the peninsula. b) Aerial firefighting efforts to contain the extent of the wildfires. Buckets of freshwater were dropped using helicopters for fire suppression. c) The thick smog around the eruption site created from mixing between wildfire and volcanic emissions. Either side of the road areas of scorched earth from moss that has already burnt can be seen. d) Satellite image adapted from Landsat 9 – OLI-2 on 17th July 2023 showing the extent of moss burning and lava flows across the Reykjanes Peninsula, Iceland, during the Litli-Hrútur eruption (from NASA Landsat Image Gallery (Voiland, 2023)). Photos in a), b), and c) taken by L. Wainman.

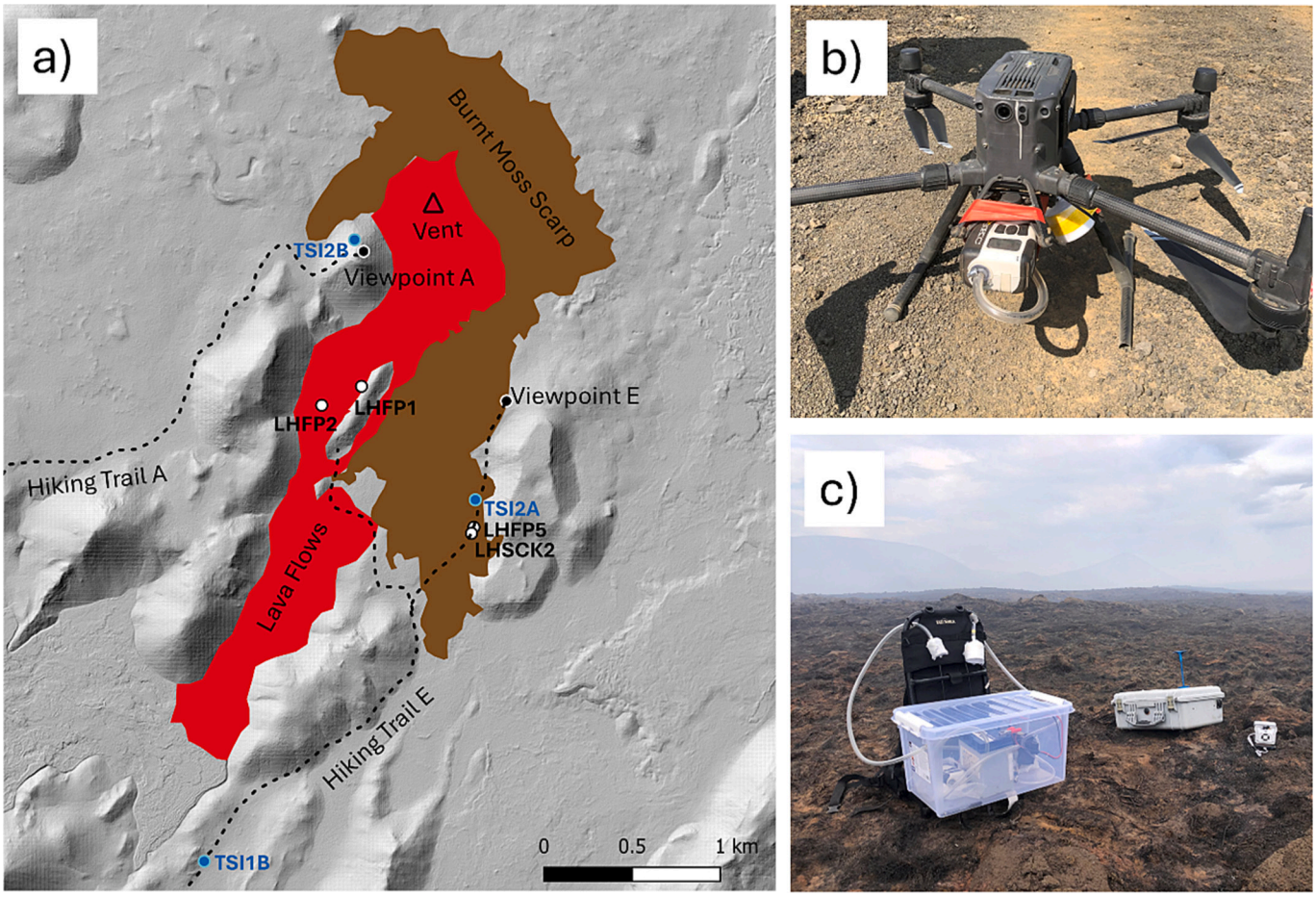

Fig. 2. The Litli-Hrútur Eruption Map and Sampling Set Up. a) Map of the Litli-Hrútur Eruption. Red infilled area shows the final extent of lava flows and the triangle marks the location of the main eruptive crate. Brown infilled area shows the total area of moss burned by lava-ignited wildfires based on satellite imagery and Schiffmann et al., 2025, Fig. 4a. Dashed lines show the official tourist hiking trails to eruption viewpoints. Note Hiking Trail E runs directly through an area of burnt moss. White circles show the locations of filter pack and cascade impactor samples and blue circles show the locations of optical particle spectrophotometer (OPS) measurements labelled according to the sample names outlined in Table 1. b) UAV-mounted sampling set up with filter pack, pump, and tubing mounted on the underside of the UAV. c) ground-level sampling on the Hiking Trail E path during active moss burning in the area. A filter pack (LHFP5), a cascade impactor (LHSKC2), and an OPS measurement (TSI1B) were collected simultaneously at this location. Photos b) and c) taken by L. Wainman.

Table 2
Optical Particle Spectrophotometer Measurements[1].

Sample ID	Sample Location	Sample Duration	Sample Type
TSI1B	Hiking Trail E	15 mins	Far-field Mixed
TSI2A	Hiking Trail E Moss Burning	45 mins	Moss Burning
TSI2B	Viewpoint A	15 mins	Near-field Mixed

[1] Measurements were collected on 16th July 2023 as part of an emergency air quality monitoring campaign with the Icelandic Meteorological Office. See Fig. 2a for exact sample locations. The 15-min average time series for OPS measurements are shown in Figs. 6, 7, and Supplementary Fig. S3.

glass and dust, see Butwin et al., 2020) and a minimum density of 1.1 g/cm^3 (wildfire smoke), with sulfate aerosol also falling between these two values (1.7 g/cm^3). Note also that the OPS used was not configured for a size bin cutoff at 2.5 μm (Bin 10: 2.156 μm - 2.685 μm) and thus we include Bin 10 in our $PM_{2.5}$ calculation, meaning this represents a slight overestimation. See supplementary datasheet S6–8 for raw particle number count data.

2.2. Sample analysis

2.2.1. Filter extraction and compositional analysis

Details of the two-stage filter extraction method are provided in the supplementary document and follow the procedures outlined in Ilyinskaya et al., (2021) and Wainman et al. (2024a). PM filter samples and blanks were analysed for major and trace elements by ICP-MS/MS in the School of Environment, Earth and Ecosystem Sciences at the Open University, UK. Synthetic calibration standards were doped with the same solution matrix as samples to eliminate ionization effects (particularly with samples containing propan-2-ol). Ionization effects were monitored by running an internal standard throughout all measurement sessions. Elements were analysed using a triple quadrupole set up with different collision gas modes (no gas, O_2, and NH_3) to minimize polyatomic and isobaric interferences (Balcaen et al., 2015; Cox et al., 2019). This allows for lower detection limits and improved accuracy across the range of elements analysed. Field, laboratory, and filter blanks were used to quantify the level of contamination at all stages of the sampling and extraction process and were found to be negligible (see Supplementary material in Wainman et al., 2024a).

2.2.2. SEM imaging and EDS analysis

The sections of filter that were not subject to the 2-stage extraction for ICP analysis (7–14 wt% of the initial filter) were examined using Scanning Electron Microscopy (SEM) and Energy Dispersive X-ray Spectroscopy (EDS) at the Leeds Electron Microscopy and Spectroscopy Centre (LEMAS), University of Leeds, UK. These small sections of filter were mounted on an aluminium stub with a sticky carbon backing, and

graphite glue was used to tack down filter edges. Mounted filters were coated with 15 nm of Pt, where Pt was chosen over C so that C-compounds in the sample could still be qualitatively identified using EDS analysis. The PTFE filter used to collect PM is composed of C, O, and F (blank filter EDS spectra shown in Supplementary Fig. S4).

SEM imaging was performed on a W-filament Tescan VEGA3 XM coupled with an X-max 150 SDD EDS detector at LEMAS at the University of Leeds, UK. An accelerating voltage of 20 kV was used for the silicate PM and 15 kV for the non-silicate organic PM, with a beam intensity between 10 and 13. Secondary electron (SE) imaging was used as it provided the greatest contrast between the particles and background filter, where SE imaging provides high resolution details on surface topography. By contrast, it was harder to differentiate between particles and the background filter when using Backscattered Electron (BSE) imaging as the particles and filters often had similar C-rich compositions.

Point-by-point EDS analysis was conducted and processed using the Aztec 3.3 Software (Oxford Instruments, UK), with a process time of 4 and an acquisition time between 45 and 120 s. Over 50 particles per sample were imaged and analysed via EDS to provide context to the morphological data collected using SE imaging. Interaction volumes for PM of different compositions (sulfate and chloride aerosol, basaltic glass, and an organic matrix representative of the moss fragments) were modelled using the CASINO software (Hovington et al., 2006) and varied between ~1 μm and 3.5 μm (see Supplementary Figs. S5a-S5d). As such, when analysing particles <3 μm in diameter via point EDS analysis the interaction volume of the beam sometimes exceeded the size of the particle. This meant that the EDS spectra showed peaks for C, O, and F which reflected interactions from the background filter. Combined with the fact that samples show significant topography (Fig. 3), EDS data is considered qualitatively.

2.2.3. TEM imaging and EELS analysis

Following SEM analysis, a single moss fragment was identified in sample LHFP1 for further analysis using Transmission Electron Microscope (TEM) Electron Energy Loss Spectroscopy (EELS). A section of this fragment (~ 10 × 18 μm) was cut out from the filter using a Focussed Ion Beam (FIB) instrument (FEI Helios G4 CX DualBeam, LEMAS, University of Leeds, UK). This fragment was then soldered to a needle and transferred to a TEM stub, to which it was then soldered using a Pt strip. The FIB gallium beam was then used to mill two sections of the sample down to the required thickness of ~100 nm, where electron transparency is needed to perform subsequent TEM-EELS analysis. The limited structural integrity of the moss particle meant that the milling process was especially delicate and that the end thickness of the sample was slightly higher in some sections (101–141 nm).

The moss fragment was then analysed by EELS on a TEM (FEI Titan3 Themis 300) at LEMAS, University of Leeds, UK. Several transects were performed along the milled sections at discrete points from the edge to the interior of the moss particle (at ~0, 0.5 μm, and 2 μm depths). Mass fractions were measured for 10 different elements, including S, Cl, K, Fe, Ca and Al.

3. Results

3.1. Particle morphologies and mixing interactions

The PM collected on filter packs around the eruption site have distinctive morphologies and size distributions depending on if the sample was collected above an outgassing lava flow, in regions of smouldering moss, or in areas of mixing between emissions, respectively (see Fig. 3 for SEM-SE images of PM). PM from outgassing lava flows (Fig. 3a – 3c) was dominated by silicate material and generally comprised of shards or blobs smaller than 30 μm in diameter. Fig. 3a shows a shard of basaltic silicate glass from sample LHFP2, that was collected above an outgassing lava flow. Fig. 3b and c show an augite crystal and glassy bead with prismatic and blob-like morphologies, respectively. This material was collected in sample LHFP1 at the lava moss-contact. The EDS spectra for the augite crystal in Fig. 3b (Supplementary Fig. S6) also contained peaks in S and Cl, possibly representing the smaller non-silicate aerosol component outgassed from the lava which is coating the surface of the particle, although the interaction volumes (1–3 μm, See supplementary Fig. S5) meant that it was not possible to perform EDS analysis on these sub 1 μm particles, despite their known abundance in volcanic plumes (Martin et al., 2008; Mather et al., 2012). The background filter of sample LHFP1 also showed EDS peaks in S and Cl, indicating a widespread dispersal of these small size-fraction S and Cl-rich secondary volcanic aerosols across the filter (Supplementary Fig. S7).

Figs. 3d-e show examples of the particles generated by the moss-wildfire burning. These are characaterised by large (> 100 μm length) moss fragments with fibrous textures (Fig. 3d-e) which have likely been disarticulated upon burning and atmospheric transport. Point EDS analysis showed that these particles are C and O-rich but some also had minor peaks in S and Cl (e.g., Supplementary Fig. S8). Fragments of additional biological material were also present in this sample, which was collected above areas of active smouldering and burnt soil. Fig. 3f shows the siliceous test of a Testate amoeba, which is a unicellular amoeboid protist that is commonly found in freshwater environments, including lakes and rivers, as well as peat bogs, moss, and soils (Opravilová and Zahrádková, 2003). The tests are very resistant even after the amboeba has died, so it is possible that the test was remobilised from the soil into the atmopshere during the wildfire burning along with other organic material (Perron et al., 2022).

Figs. 3g-i show volcanic and wildfire particulates that have interacted upon emission directly at the lava-moss burning interface. Figs. 3g-h show the moss fragments associated with multiple similarly sized silicate fragments to form a larger agglomeration of mixed particles. These agglomerations have total diameters >60 μm which is much greater than the <30 μm diameters generally seen for individual silicate shards. The size difference between the larger moss fragments (> 100 μm length) and smaller silicate shards can also be seen in Fig. 3i in sample LHFP1, containing mixed volcanic and wildfire PM collected above burning at the lava-moss interface. Differences are also seen between the composition of an unused blank filter and the background of the filter collected at the moss-lava interface which had a higher relative C peak and the apperance of being covered in a sticky film.

Agglomeration is especially pronounced in sample LHFP5, which was collected on Hiking Trail E, downwind of both the volcanic vent and area of lava-moss burning at the time of sampling. Fig. 3j shows a cluster of silicate fragments of varying sizes that have clumped together to form a larger agglomeration, possibly during atmospheric transport and collisions. Fig. 3k-3l show larger moss particles with many smaller silicate shards and S and Cl-rich particles stuck to/inbetween the C-rich fibres that comprise the moss particle. Across this sample (LHFP5) the majority of large fibrous moss fragments were similarly covered in smaller volcanic aerosol particulates.

3.2. Particle coating and gaseous interactions

As highlighted above, some of the moss particles that were burnt directly at the interface with advancing lava flows (LHFP1) also had minor peaks in S and Cl when analysed by EDS point analysis (Supplementary Fig. S8). SO_2 and HCl are major componenents of volcanic degassing (Aiuppa, 2009; for the Fagradalsfjall eruptions see Halldórsson et al., 2022 and Wainman et al., 2024b), and so these peaks in S and Cl may be indicative of the organic moss particles interacting with volcanic gases as it is co-transported in the mixed plume. To invesitigate this possibility further we used the FIB to isolate a section of one moss particle from LHFP1 (lava-moss interface sample) that showed EDS peaks in S and Cl. This fragment was then transferred to the TEM instrument where we performed EELS analysis across two transects from

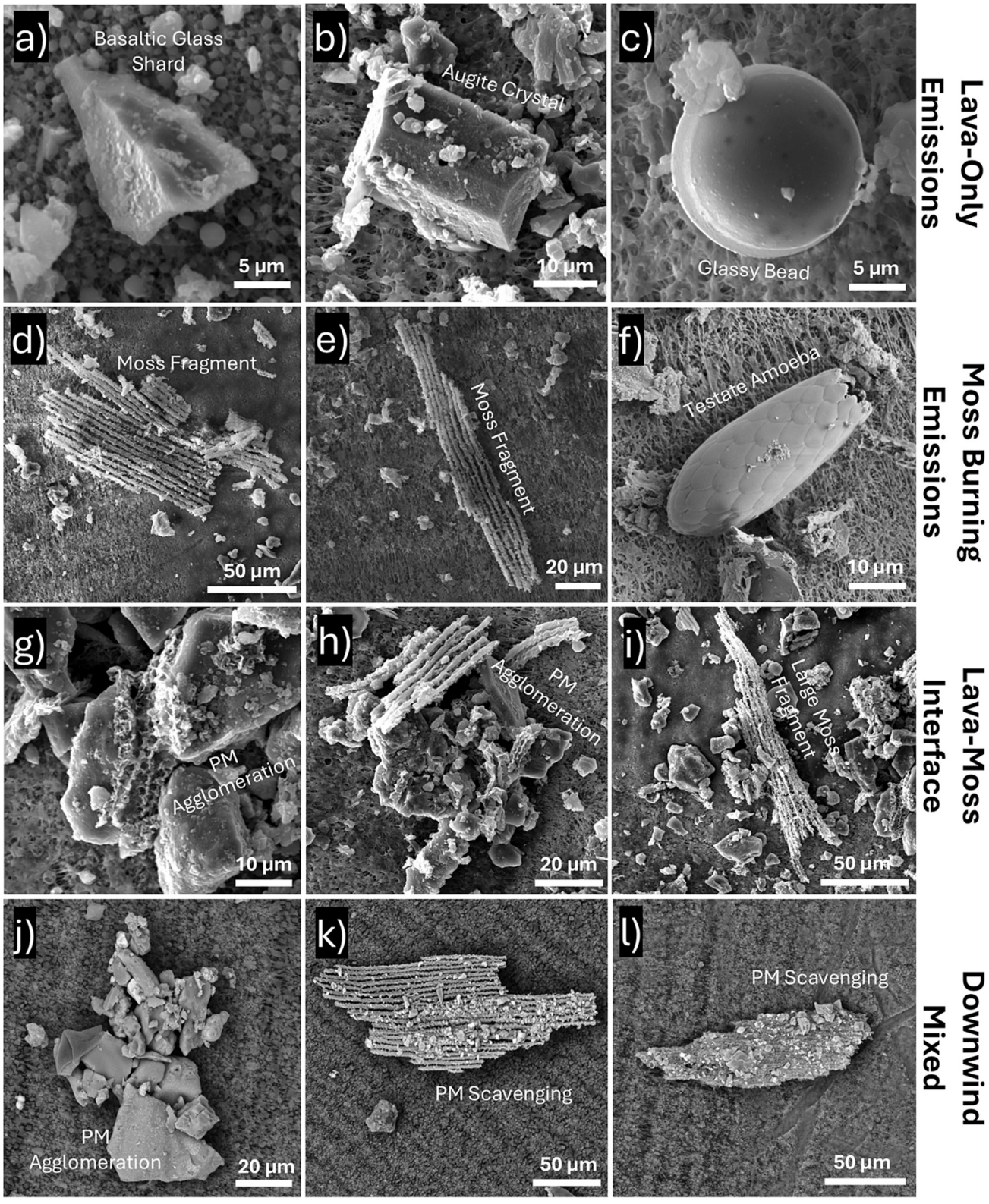

Fig. 3. SEM-SE Images of Lava, Wildfire, and Hybrid PM from filter pack samples. a) Angular silicate shard from outgassing lava sample LHFP2. b) Prismatic Fe silicate particle identified as augite by EDS from the mixed lava-moss sample LHFP1. c) Al—Ca silicate blob also from LHFP1. d-e) Fibrous C-rich moss fragments from mixed moss-lava sample LHFP1, similar to images in Robinson (1971). Mosses were likely disarticulated during burning and some fragments displayed S and Cl peaks in EDS analysis. f) Test from a Testate amoeba from sample LHFP1, remobilised from the soil during wildfire burning. g) Moss fragment binding together two silicate shards (LHFP1). h) Agglomeration of silicate shards and C-rich moss fragments (LHFP1). i) Larger moss particle surrounded by smaller silicate PM (LHFP1). j) Agglomeration of silicate shards in downwind ground-level sample LHFP5 from Hiking Trail E. k-l) Large moss particles with smaller silicate shards stuck between fibres of the moss particle.

the surface to the interior of the moss particle at three distinct points: 1) Moss surface, as close as possible to the edge without touching the Pt bar souldered across the top, 2) Moss sub-surface, ~ 500 nm depth from the surface, 3) Moss interior, ~ 2 μm from the moss surface layer. EELS analysis reported the mass fraction of 10 different elements, including refractory elements Al, Ca, and Fe, as well as the relatively more volatile elements S, Cl, and K.

The mass fractions of the refractory elements Al,Ca, and Fe remain within analytical error across all three locations from the surface-to-edge transect, suggesting there is no significant variation in the behaviour of these elements throughout the width of the moss particle (Fig. 4 and Supplementary Table S1). By contrast, mass fractions of S and Cl, which are potentially indicative of interactions with volcanic gases, SO_2 and HCl, are within error of each other at the particle surface and sub-surface, but mass fractions from the interor are significantly lower (See Fig. 4 and Supplementary Table S1). The mass fractions of S and Cl do not show a single discrete layer solely on the surface of the moss particle, but also appear elevated within the subsurface. The mass fraction of K, which is known to be a volatile trace element with a tendency to form chlorides in volcanic gases (Mather et al., 2012; Mason et al., 2021), follows a similar pattern to S and Cl, where the mass fraction of K is highest at the surface of the moss particle, also within error of the subsurface, but is significantly higher than in the mass fraction of K in the interior of the moss particle.

3.3. Trace element signatures

PM samples collected by filter pack at the lava-moss interface (LHFP1), above an outgassing lava flow (LHFP2), and on the downwind hiking path, where volcanic and wildfire emissions were mixing in the atmosphere (LHFP5), all have distinct trace element signatures. Fig. 5a shows the concentrations of a range of trace elements collected at the lava-moss interface (LHFP1), normalized to the concentration of the same elements collected above an outgassing lava flow (LHFP2). Elements are ordered on the x-axis by increasing values to the right, where all elements have higher concentrations in the lava-moss interface sample compared to the lava-only outgassing emissions. The elements which are most in enriched in the lava-moss interface sample compared to the lava-only outgassing are thus likely derived from an additional vegetation burning contribution to the overall aerosol composition and include Mg, Ca, Zn, Sn, Ba, K, P, and Sb. Ca, Mg, Ba, K, and P are essential macronutrients in plants, whilst Zn is an additional micronutrient (Grusak et al., 2016). Sn and Sb can be toxic in plants in high concentrations but are commonly taken up from soils, particularly if soils are contaminated by transport or industrial pollution or if leaching has occurred from sulfide rich rocks (Tang et al., 2022). Elements on the left-hand side of Fig. 5a by contrast show lower enrichment in the lava-moss interface emissions relative to stand-alone lava outgassing and include elements which are known to be hosted in both the primary (La, Ce, Ta) and secondary (Tl, Ag, Se, Cs, Te, Cd, Cu, As, Pb) volcanic aerosol phase. The slightly greater enrichment of elements found in the primary volcanic aerosol (silicate ash; La, Ce, Ta) compared those in the secondary volcanic aerosol (volatile trace elements; Tl, Ag, Se, Cs, Te, Cd, Cu, As, Pb) suggests a somewhat greater ash component was collected on the LHFP1 PM filter compared to LHFP2, possibly resulting from sampling at different positions along the lava flow; Sample LHFP1 was collected above an actively burning A'ā lava front, which possibly had a greater emission of silicate PM compared to LHFP2 which was collected above a more effusively outgassing Pāhoehoe lava flow.

Fig. 5b shows trace element concentrations collected in sample LHFP5 on Hiking Path E normalized to the concentration of the same elements collected above outgassing lava flow sample LHFP2. Element concentrations in the downwind mixed sample (LHFP5) are much lower than in both the outgassing lava sample and at the lava-moss interface. This is most likely because of mixing with the ambient atmosphere and downwind dilution of the mixed volcanic-wildfire plume. In Fig. 5b the elements on the x-axis are presented in the same order as in Fig. 5a for comparison. Generally, elements follow a similar trend as Fig. 5a with increasing enrichment over the lava outgassing sample towards the right-hand side of the plot. Nonetheless, some elements deviate from the trend of increasing concentration towards the right in Fig. 5b. For example, Cs, Cu, As, Pb, La, Ce, Sn, and Sb are higher in concentration in the downwind mixed sample compared to the lava-moss interface sample than might be expected based on Fig. 5a showing a general trend of increasing enrichment towards the right. This suggests that the two samples, at the lava-moss interface and the downwind mixed plume, are not simply related by homogenous downwind atmospheric dilution, which would preserve this increasing-rightward pattern, but that other processes such as selective deposition or scavenging may be contributing to a fractionation in the trace element concentrations in the downwind plume.

Alongside distinctive geochemical compositions, PM from the lava-

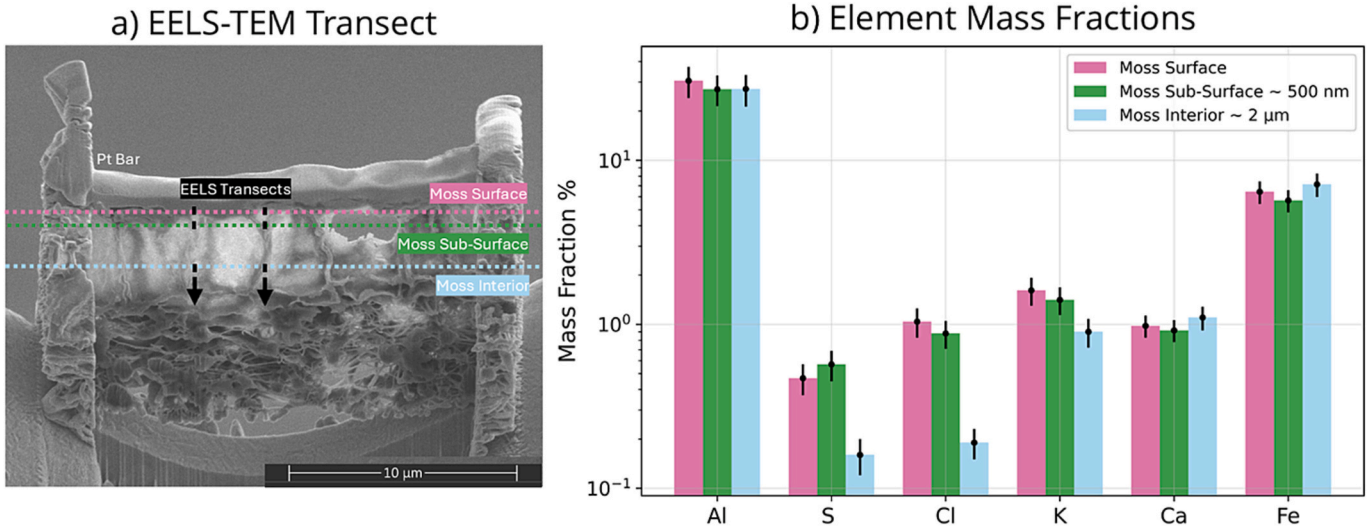

Fig. 4. TEM Image and EELS Transects with Mass Fraction % for a Selection of Elements. a) Image of the moss fragment that was cut out from SEM mounted sample LHFP1 using a FIB, before being milled down to electron transparency (approximately 100 nm). Schematics of the TEM-EELS transects are shown, which were performed across two sections of the fragment at three discreet depth locations: 1) Surface, 2) Sub-surface (~ 500 nm depth), 3) Interior (~ 2 μm). b) Mass fractions for a selection of refractory (Al, Ca, Fe) and volatile (S, Cl, K) elements. Black lines show the mass fraction analytical error bars.

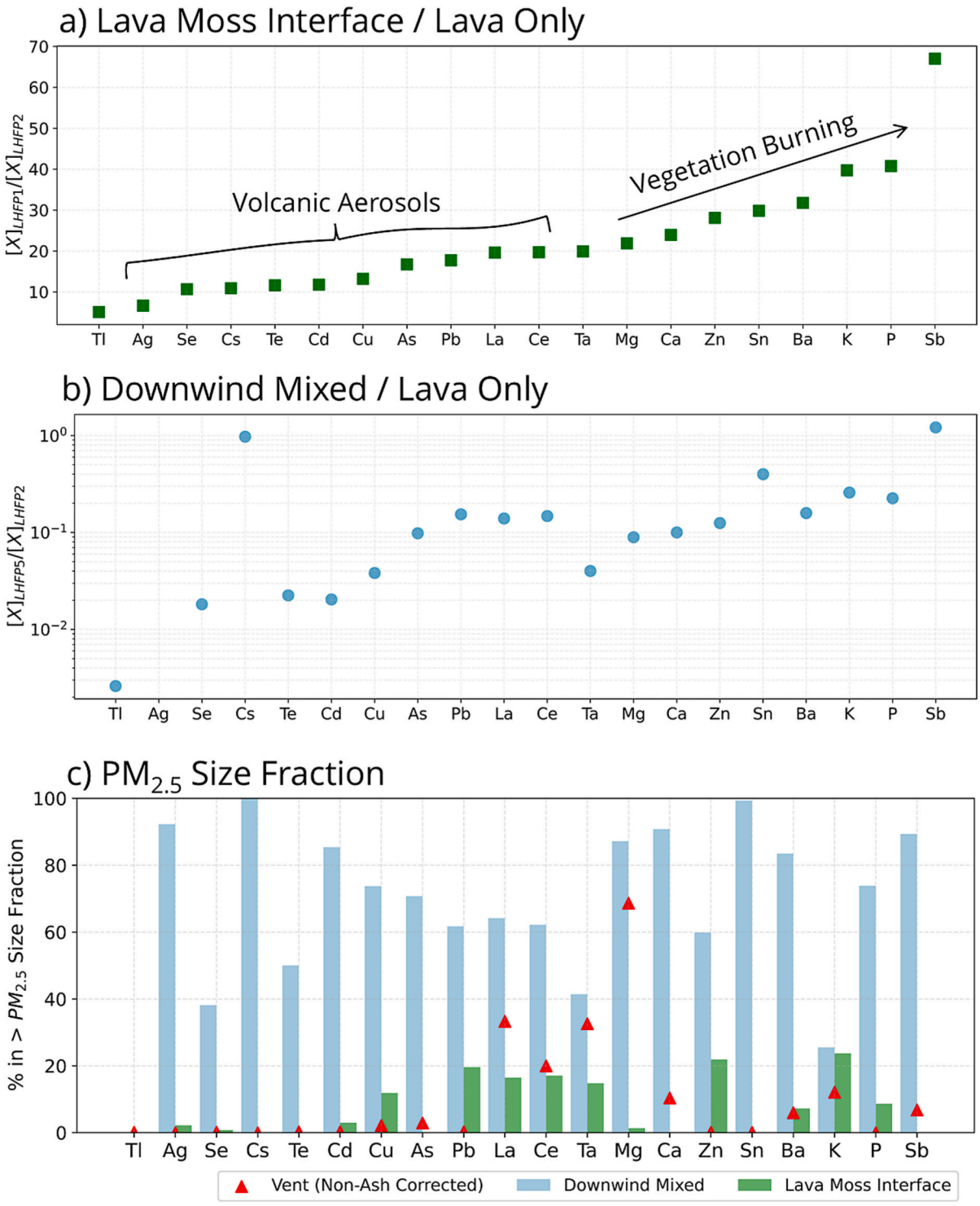

Fig. 5. Trace Element Signatures and Size Distributions in PM samples. a) Element filter concentrations in sample LHFP1 (lava-moss interface) normalized to element concentrations in sample LHFP2 (lava outgassing). Elements are ordered on the x-axis from left to right by increasing enrichment in the lava-moss interface sample compared to the lava outgassing sample. b) Element filter concentrations in sample LHFP5 (mixed downwind sample, Hiking Path E) normalized to element concentrations in sample LHFP2 (lava outgassing). Elements are ordered on the x-axis as in panel a). c) Proportion of each element hosted by mass in the >2.5 μm component, as measured using a cascade impactor in samples from the lava-moss burning interface (Green bars; LHSKC1), in the downwind mixed sample (blue bars; LHSCK2), and from an end-member volcanic vent sample (red triangles; LHSKC3) Note the most refractory elements such as Ce, La, Mg, Ba, and Ca are likely to be under sampled by the SKC impactors (Wainman et al., 2024b).

moss interface and in the downwind mixed plume sample show distinctive element concentrations associated with particle size distributions. Fig. 5c shows the percentage of each element by mass collected in the > $PM_{2.5}$ size bin using a cascade impactor. Elements at the lava-moss burning interface (green bars) are predominantly contained within the <2.5 μm fraction (no element is more than 25% by mass in the >2.5 μm impactor stages), and it is only a subset of elements which have any component in the >2.5 μm size bin (Ag, Cd, Cu, Pb, La, La, Ta,

Mg, Zn, Ba, P, K). Elements collected in the downwind mixed emissions on Hiking Trail E show, by contrast, much higher proportions in the >2.5 μm size bin across nearly all elements: Cu, Pb, La, Ce, Ta, Zn, Ba, K, and P, which had <25% in the >2.5 μm component at the lava-moss interface all have over 25% in the >2.5 μm component in the Hiking Trail E sample. In addition, elements such as Ag, Se, Cs, Te, Cd, As, and Sn, which had negligible > $PM_{2.5}$ components in the lava-moss interface sample, have between 30 and 100% by mass in the > $PM_{2.5}$ component in the downwind mixed plume sample. The proportion of each element hosted in the >2.5 μm size fraction from a volcanic vent cascade impactor sample is also presented on Fig. 5c (red triangles) to allow comparison with a volcanic endmember. Within the volcanic vent sample, the trace elements fall into two distinct categories: 1) volatile trace elements which are hosted almost entirely in the <2.5 μm fraction and 2) refractory trace elements which are hosted in the primary silicate ash and have a greater proportion by mass in the >2.5 μm fraction (Martin et al., 2008; Mather et al., 2012). Supplementary Fig. S9 presents a comparison of ash corrected vs non-ash corrected at-vent element concentrations to further highlight which elements are predominantly derived from the primary silicate ash phase.

3.4. Bulk size distribution and OPS reprocessing

During the air quality monitoring campaign on the 16th of July 2023, we carried out an exploratory assessment using an OPS to measure concentrations of PM_{10} and $PM_{2.5}$ at different locations around the eruption site. Fig. 6 shows a timeseries of $PM_{2.5}$ and PM_{10} concentrations over a 15-min sampling window recorded on Hiking Trail E and Fig. 7 shows $PM_{2.5}$ and PM_{10} timeseries over a 15-min window at Viewpoint A (see Fig. 2a for sampling map). Fig. 8 and Fig. 9 show 15-min average box plot distributions of $PM_{2.5}$ and PM_{10} concentrations, respectively. The traffic light system used in Figs. 8 and 9 follows the classification of health hazard level used by the Icelandic Environment Agency for 1 hr exposure limits (Table S2, Icelandic Environment Agency, 2025). Whilst 1 hr exposure limits do exceed our sampling window (15 mins) they were used for reference as they are the closest existing air quality thresholds, are most representative of the acute nature of potential exposure where tourists were hiking for several hours, and the most relevant for informing Icelandic civil protection agencies.

$PM_{2.5}$ concentrations varied significantly between Hiking Trail E and Viewpoint A. Over the 15-min sampling window Hiking Trail E had lower average $PM_{2.5}$ concentrations whilst at Viewpoint A $PM_{2.5}$ concentrations were generally higher over the 15-min sampling window (See Fig. 8 and Table 3). Based on the Icelandic Environment Agency 1 h exposure thresholds this places Hiking Trail E within the Yellow category whereas Viewpoint A falls one category above, in Orange. The distribution of $PM_{2.5}$ concentrations also varied between sampling locations; at Hiking Trail E there is a wider range of values, although most fall within the lower end of the distribution (< 10 $\mu g/m^3$ see Figs. 6 and 8). This suggests the mean and median values are pulled up by discrete but short-lived peaks in concentration, and such peaks can be seen in the timeseries shown in Fig. 6. The largest peak in $PM_{2.5}$ at Hiking Trail E reaches >100 $\mu g/m^3$, with a total of ~4.4 min (29% of sampling period) spent in the Orange or Red exposure thresholds over the 15-min sampling window. At Viewpoint A, by contrast, the distribution of concentrations is tighter, not decreasing below 8 $\mu g/m^3$ across the whole sampling period, and with most of the values falling in the Orange category (See Figs. 7 and 8). This suggests that $PM_{2.5}$ values at Viewpoint A were instead more consistently elevated rather than occurring in discrete peaks with 12.2 min (81%) of the 15-min sampling period exceeding the Orange exposure threshold.

PM_{10} concentrations show similar variations between Hiking Path E and Viewpoint A, where average concentrations on Hiking Trail E are lower compared to Viewpoint A. These values place them in the Dark Green and Light Green thresholds respectively. PM_{10} concentrations also show similar distributions to $PM_{2.5}$ at both Hiking Trail E and Viewpoint A. Hiking Trail E generally has lower values punctuated by very high peaks (the highest peak in PM_{10} is coincident with the highest peak in

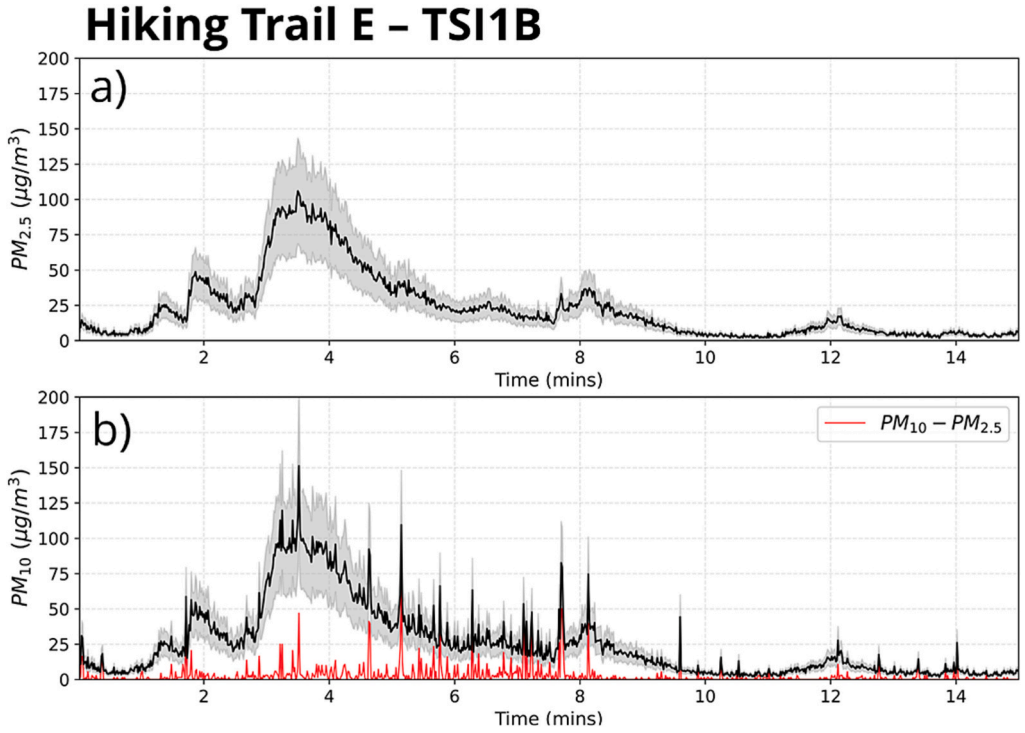

Fig. 6. Timeseries of OPS PM data collected at Hiking Trail E (TSI1B) across a 15-min sampling window. Solid black line shows concentrations with an assumed uniform density of 1.7 g/cm^3 (sulfate) and the shaded area shows upper and lower estimates with assumed densities of 1.1 g/cm^3 (smoke) and 2.3 g/cm^3 (glass), respectively. Red line shows $PM_{10} - PM_{2.5}$ to isolate the coarser fraction contribution to PM_{10}. Other assumptions are outlined in Section 2.1.4. Raw particle count data is included in Supplementary Sheet S6.

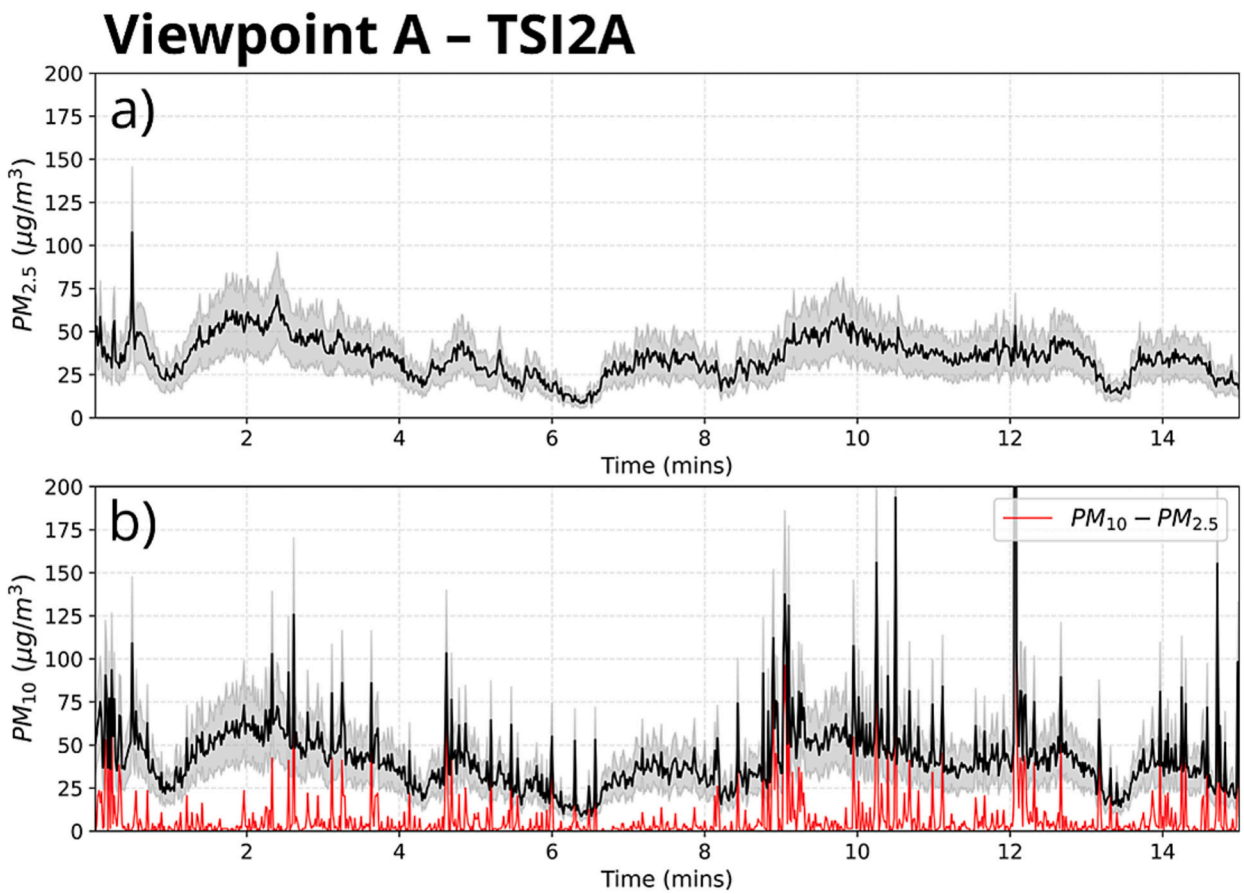

Fig. 7. Timeseries of OPS PM data collected at Viewpoint A (TSI2B) across a 15-min sampling window. Solid black line shows concentrations with an assumed uniform density of 1.7 g/cm^3 (sulfate) and the shaded area shows upper and lower estimates with assumed densities of 1.1 g/cm^3 (smoke) and 2.3 g/cm^3 (glass), respectively. Red line shows $PM_{10} - PM_{2.5}$ to isolate the coarser fraction contribution to PM_{10}. Other assumptions are outlined in Section 2.1.4. Raw particle count data is included in Supplementary Sheet S8.

$PM_{2.5}$ and reaches 110 μg/m^3). As shown by the red line on Fig. 6, the baseline PM_{10} concentrations at Hiking Trail E are mostly comprised of the <2.5 μm fraction ($PM_{2.5}$), which is then punctuated by discrete and generally small peaks containing a coarser (2.5 μm – 10 μm) component. Viewpoint A by contrast has consistently higher but less variable PM_{10} concentrations (See Fig. 7 for 15-min concentration time series). Fig. 7b shows that baseline PM_{10} concentrations at Viewpoint A are still dominated by the <2.5 μm fraction, but there are larger and more regular peaks in the coarser PM_{10} fraction (2.5 μm – 10 μm). Between Hiking Trail E and Viewpoint A the degree of correlation also varied between $PM_{2.5}$ and PM_{10}: at Hiking Trail E $PM_{2.5}$ and PM_{10} show a strong positive degree of correlation whereas at Viewpoint A there is only a weak positive correlation (Table 3). Fig. S3 in the Supplementary Material shows $PM_{2.5}$ and PM_{10} concentrations measured further along Hiking Trail E in an area of active moss burning (TSI2A). This measurement shows exceptionally high concentrations of $PM_{2.5}$ (average of 805.6 μg/m^3) and PM_{10} (average of 848.3 μg/m^3), with concentrations of both $PM_{2.5}$ and PM_{10} remaining in the Red category throughout the sampling window. Whilst collecting these measurements, the OPS was placed on the ground within 2–3 m of actively smouldering moss and directly downwind of the resulting smoke. This measurement therefore represents endmember at-source concentrations of PM_{10} and $PM_{2.5}$ during moss wildfire burning, rather than what is likely to be inhaled by people (or animals) following dilution during downwind transport.

4. Discussion

4.1. Formation of hybrid particulate matter

Lava flow outgassing and wildfire burning produced physically and chemically distinct emissions of gas and PM, however, upon mixing between end-member emissions, either directly at the burning interface or during downwind atmospheric transport, mechanical interactions between gaseous and particulate species resulted in the formation of hybrid PM with altered physicochemical characteristics. In this section, we discuss the primary mechanisms that contributed to the formation of hybrid PM and highlight how these processes may have resulted in the alteration of the physical and chemical characteristics of some hybrid PM compared to endmember volcanic and wildfire emissions.

Directly at the lava-moss burning interface, SEM imaging showed that fibrous moss fragments can in some instances stick together with similarly sized silicate shards to form larger agglomerations with increased diameters relative to the individual particles. Figs. 3g – 3h show examples of these agglomerations of volcanic silicate shards, held together by carbonaceous fragments of partially combusted moss. The process of particle agglomeration is well documented in volcanic settings, for example, as volcanic ash aggregation in explosive plumes (Brown et al., 2012) and via aerosol coagulation (Ammann and Burtscher, 1993). In both instances, aggregation and coagulation contribute to particle growth and an increase in the overall PM size distribution. The agglomeration of volcanic silicate PM with the partially combusted moss particles observed for some particles in this study likely occurred via Brownian motion and impaction close to the

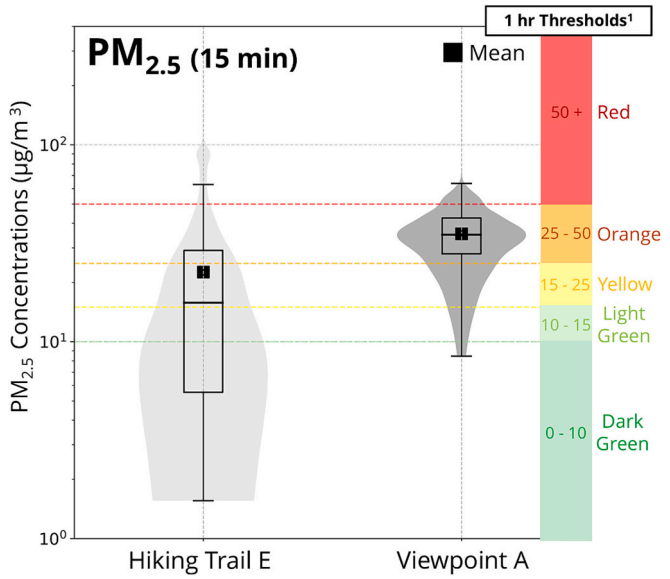

Fig. 8. $PM_{2.5}$ Concentrations at Hiking Trail E and Viewpoint A. Concentrations were measured during a 15-min sampling window with an optical particle spectrophotometer and calculated with an assumed uniform density of 1.7 g/cm^3. Box and Whisker plot shows the median, first quartile (Q1; 25th percentile), third quartile (Q3; 75th percentile), minimum (Q1–1.5*interquartile range, IQR) and maximum (Q3 + 1.5*IQR). Filled black square shows the mean concentration over the 15-min sampling interval. Shaded violin plots show the distribution of the concentration data across the 15 min, smoothed by a kernel density estimation, which represents the probability of a given value. [1]The right-hand traffic light system corresponds to the air quality classification scheme used by the Icelandic Environment Agency for 1 h exposure thresholds (Icelandic Environment Agency, 2025, full details in Supplementary Table S2). Raw instrument particle count data are included in Supplementary Sheets S6 and S8 and concentration timeseries are included in Figs. 6 and 7.

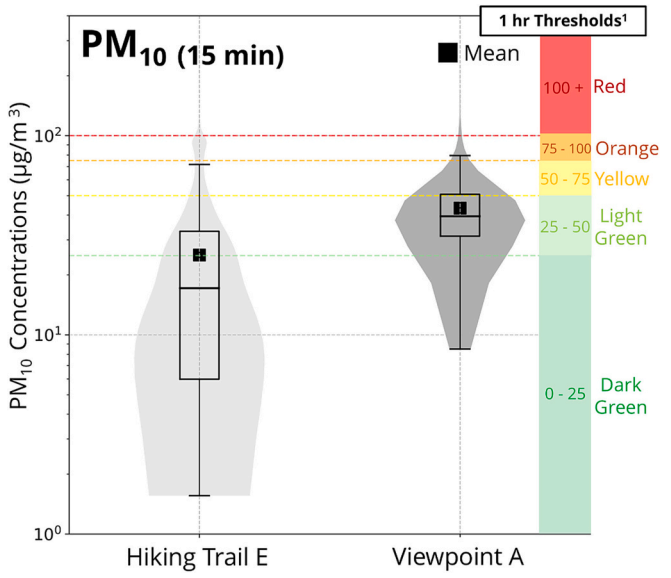

Fig. 9. PM_{10} Concentrations at Hiking Trail E and Viewpoint A. Concentrations were measured during a 15-min sampling window with an optical particle spectrophotometer and calculated with an assumed uniform density of 1.7 g/cm^3. Box and Whisker plot shows the median, first quartile (Q1; 25th percentile), third quartile (Q3; 75th percentile), minimum (Q1–1.5*Interquartile Range, IQR) and maximum (Q3 + 1.5*IQR). Filled black square shows the mean concentration over the 15-min sampling interval. Shaded violin plots show the distribution of the concentration data across the 15 min, smoothed by a kernel density estimation, which represents the probability of a given value. [1]The right-hand traffic light system corresponds to the air quality classification scheme used by the Icelandic Environment Agency for 1 h exposure thresholds (Icelandic Environment Agency, 2025, full details in Supplementary Table S2). Raw TSI particle counts are included in Supplementary Sheet S6 and S8 and concentration timeseries are included in Figs. 6 and 7.

emission interface. Whilst this represents a similar process to those already documented, agglomeration between two separate emission sources is unique to this compound volcanic-wildfire event. Nonetheless, it is important to note that the Litli-Hrútur compound volcanic-wildfire presented in this study represents only one example and may be specific to the regional vegetation of Iceland. Burning of other types of organic matter (e.g., forests or grasslands) may result in differing agglomeration mechanics.

TEM-EELS analysis (Section 3.2) also suggests that there may be interactions between volcanic gaseous species, such as SO_2 and HCl, and the moss PM as it is burnt at the interface with the advancing lava flow. A moss particle from the lava-moss burning interface showed higher concentrations of S and Cl nearer the surface relative to the interior, which had negligible mass concentrations of S or Cl (Fig. 4). We interpret the enrichment of S and Cl only at the surface of the moss particle to suggest that they were most likely derived from an external airborne source, rather than through uptake from the soil, especially as terrestrial mosses have a particularly high airborne adsorption capacity (Varela et al., 2023). Mosses can take up species from the atmosphere either via precipitation (wet deposition) or by capturing airborne particles (dry deposition) on their highly porous surfaces (Varela et al., 2023). Nonetheless, without a sample of unburnt moss which grew in proximity to the previous eruptions, there remain two possible scenarios to explain the peaks in S and Cl: 1) volcanic gases and volatile trace elements are taken up prior to the wildfires when the moss was growing in proximity to previous active eruptions, or 2) interactions with volcanic gases and aerosols occurred after burning and subsequent plume mixing during atmospheric transport. The EDS peaks in S and Cl on the background filter of sample LHFP1 favour the latter possibility as they must have

Table 3
Statistical details for OPS measurements.

	Hiking Path E		Viewpoint A	
	$PM_{2.5}$	PM_{10}	$PM_{2.5}$	PM_{10}
Mean	22.6	25.2	35.5	43.3
Median	15.8	17.2	34.9	39.4
IQR	23.5	27.1	14.5	19.5
Pearson R Coefficient	0.97 $p < 0.05$		0.37 $p < 0.05$	

occurred *syn*-transport in the mixed plume, although do not exclude an additional contribution of S and Cl taken up in the moss whilst it was growing. Both possibilities demonstrate that mosses (or possibly vegetation more generally) in volcanic environments may provide an additional pathway for the uptake and mobility of metal and trace pollutant species (e.g. Arndt et al., 2017), or in the atmosphere if fragments of this moss are remobilised in the plume upon burning. Notably several metals, such as Al, Fe, and Ca, also showed no significant variation from the surface to the interior of the moss particle during the TEM-EELS transects, whilst K, which was the only more volatile trace element we measured, showed a pattern similar to S and Cl, with much higher concentrations in the surface and subsurface compared to the interior. We hypothesise that this means the mosses are interacting not only with the primary volcanic gases SO_2 and HCl, but also the secondary volcanic aerosols which contain volatile volcanic trace elements.

As well as occurring directly at the burning interface, mixing and subsequent mechanical interactions can also occur between lava and wildfire emissions during downwind transport in the volcanic-wildfire plume. Comparison of the proportion of elements hosted in the <2.5

μm fraction between the lava-moss interface and downwind mixed samples (Fig. 5) shows that the proportion of all elements in the >2.5 μm size bin is much greater in the downwind hiking sample relative to the lava-moss interface. Given the ground-based nature of this downwind sample, this observation could represent a preferential sampling of the larger size fraction PM (including hybrid PM formed via agglomeration) which settled out more rapidly from the near vent plume and thus preferentially collected on our ground level filters whilst the smaller size fraction remained airborne at higher altitudes. However, the observed increase in the proportion of elements hosted in the >2.5 μm size fraction could also be explained by particle scavenging, which would also lead to an increase in the overall PM size distribution by the removal of the smaller <2.5 μm fraction. SEM images of the downwind filter showed that the larger partially combusted moss particles did, in some cases, act as "nets" which scavenged and removed the much smaller silicate volcanic aerosols that collected between the fibres of the moss particles (Figs. 3k – 3l). Scavenging is a well-documented process in volcanic plumes, where scavenging of volatiles such as sulfur, halogens, and trace metals, by volcanic ash is major sink of these elements from explosive volcanic plumes (Rose, 1977; Mather et al., 2003; Witham et al., 2005). Nonetheless, as with the agglomeration processes discussed above, in the context of this compound volcanic-wildfire event it is unique in occurring between emissions of different origins.

Furthermore, the agglomeration and scavenging of secondary volcanic aerosols by larger moss particles does not appear to be equally as efficient across the different metal and metalloid elements in our dataset. For example, at the lava-moss burning interface only some elements, such as Cu, Pb, Zn, and K show a significant increase in their proportions in the >2.5 μm size bin relative to volcanic-end-member emissions. We hypothesise this could suggest that they have a greater affinity to form agglomerations with or being scavenged by the moss, compared with other elements such as Se and Te which have similarly negligible proportions in the >2.5 μm component compared to volcanic end member emissions. In the downwind mixed sample, elements such as Se and Te also show a lower relative increase in the proportion collected in the >2.5 μm size bin, potentially indicating that they have less affinity for being scavenged and collected by the moss particle "nets" during downwind mixing. The fractionation in element concentrations measured in the downwind mixed sample can be partially split by differences in element speciation behaviour (Cu, Pb, Zn, and K have an affinity for forming chlorides, whilst Se and Te more commonly bond with S). It has previously been demonstrated that S-bonding and Cl-bonding gases and metals have varied affinities for wet and dry interactions in volcanic plumes, including scavenging by silicate ash particles (Rose, 1977, Witham et al., 2005, Wainman et al., 2024b).

The observed fractionation in element concentrations in the downwind ground-based sample also provides some evidence for the increase in particle size distribution being to a greater extent the result of scavenging instead of preferential sampling of selectively deposited particles. Wainman et al. (2024b) suggest that, for the same eruptions in Iceland, under dry background conditions S-bonding elements are likely to be selectively deposited from the plume faster relative to elements with an affinity for Cl. By contrast in the downwind mixed plume sample in this study it is the Cl-bonding elements which show relatively greater enrichment. This provides preliminary evidence not only for scavenging of volcanic PM by larger partially combusted moss particles as a key process in increasing the overall particle size distribution during compound events, but also that the efficiency of the scavenging process, between moss and volcanic particles, may at least in part be based on element chemical speciation. Not all elements are clearly split in their moss scavenging efficiency by a distinction in their speciation behaviour, however. For example, Sn, which generally forms a sulfide, is 100% in the >2.5 μm size bin suggesting a very strong affinity for scavenging by the moss particles. This emphasises the need to better constrain the mechanisms and underlying controls on processes such as scavenging and agglomeration in volcanic plumes, including for example, the effect of parameters such as element speciation and element water solubility.

4.2. Implications for transport, environmental dispersion, and human exposure

In this section we discuss how the scavenging and agglomeration effects and the resulting changes in PM characteristics, predominantly via increased particle size and removal of the smaller PM size fraction, may have implications for the subsequent transport and dispersion of key pollutant species in the mixed volcanic-wildfire plume. As highlighted above, agglomeration between and scavenging of volcanic aerosols by the larger moss fragments is likely to increase the size of some hybrid particles and contribute to the removal of the smaller volcanic size fraction from the mixed plume. Similarly to the effects of volatile scavenging by larger silicate ash particles and ash aggregation in explosive plumes, we propose that interactions with the moss particles are likely to contribute to the enhanced gravitational settling of 1) the larger agglomerated particles and 2) the smaller volcanic PM size fraction which are scavenged by and deposited out with the larger moss particles onto which they are stuck (Wesely and Hicks, 2000). These scavenging and agglomeration processes, which occur upon mixing between volcanic and wildfire PM, thus potentially provide an additional deposition pathway that is specific to compound volcanic wildfire events. Theoretically, enhanced deposition rates in the mixed near-vent plume could lead to more intense localised air and environmental pollution but reduced long range transport relative to a non-wildfire-inducing volcanic eruption. Given the preliminary observation that moss particle scavenging efficiency of volcanic PM may vary between different trace elements (Fig. 5), this pathway could also lead to a fractionation in element transport distances, where the elements which are most efficiently scavenging by the moss particles such as Ag, Cs, and Sn, have the greatest reduction in long range transport during compound volcanic wildfire events. By contrast, elements such as Se and Te which are less efficiently scavenged by the moss particles may experience a relatively greater degree of long-range dispersion. Crucially, this could have implications for the suite of metals to which people may be exposed in a compound volcanic-wildfire event compared to a volcanic eruption with no simultaneous wildfire.

The exposure risk for tourists and frontline workers in the vicinity of the eruption/wildfire burning area, also varied locally around the eruption/wildfire site, depending on topography, wind direction, and proximity to the different emission sources. For example, OPS measurements at Viewpoint A and Hiking Trail E highlight the considerable local variability in PM concentrations, where Viewpoint A was in closer proximity to both wildfire burning and emissions from the volcanic vent and lava flows and thus had on average high PM concentrations. Viewpoint A also had a topographic high to the rear which may have contributed to the build-up of airborne pollution within the relative topographic low of the Viewpoint due to orographic effects. By contrast Hiking Trail E was further from the volcanic PM sources and sat within a wider and flatter plain where gusts of wind may have flushed the pollution more regularly in between high concentration peaks. In comparison to a stand-alone wildfire, it is also possible that ignition by a lava flow may alter the burn dynamics relative to a fire ignited by other sources and thus result in a different overall particle size distribution (e.g., smouldering fires generally produce coarser PM with a larger mean diameter - Pokhrel et al., 2020).

OPS measurements also show that for both locations $PM_{2.5}$ was on average in a more hazardous air pollution category (Yellow/Orange) than PM_{10} (Light Green/Dark Green) and thus may have been the predominant contributor to ground-level exposure risk. Scaling up $PM_{2.5}$ exposure (29% exceeding the orange threshold) along Hiking Path E for a 8–10 hr round trip (and assuming only half of this time was within dispersion distance of the volcanic/wildfire air pollution) corresponded to nearly an hour and a half of exposure to > Orange $PM_{2.5}$ threshold concentrations where "*Strenuous work or outdoor exercise should be*

avoided" (Table S2, Icelandic Environment Agency*)* on the day when we collected data. This means that even based on a preliminary examination of $PM_{2.5}$ concentrations the Icelandic Civil Defence closure of the area due to elevated gas and smoke pollution was likely very well justified on this day. Whilst this exposure is ultimately still relatively short-term, acute exposure to $PM_{2.5}$ has been associated with serious health problems, including heart and lung conditions, asthma attacks, and respiratory symptoms, particularly in vulnerable populations such as children or the elderly (Chen et al., 2024; Faherty et al., 2025). For frontline construction (Sigtryggsdóttir et al., 2025) and emergency response workers (such as search and rescue and the police) who were more regularly in the proximity of the eruption site, exposure to extremely high levels of $PM_{2.5}$ may have been even more severe, although this would require consistent longer-duration OPS monitoring to sufficiently to inform health advice. In these conditions, the widespread use of respiratory protection, effective at filtering out small particle size fractions, could be a suitable intervention to reduce exposure to the wildfire and mixed plume pollution and such protection could be included in future health protection guidance (Stewart et al., 2021).

5. Conclusions

The Litli-Hrútur 2023 eruption ignited the largest moss wildfires on record in recent Iceland eruptive history. This triggered a compound volcanic wildfire event with the simultaneous emission of volcanic gases and PM, as well as smoke from the moss wildfires. We collected samples of endmember and mixed volcanic and wildfire emissions and demonstrate lava outgassing and wildfire smoke were associated with PM with distinctive chemical signatures and size distributions. Where emissions mixed, either directly at the lava-moss burning interface or during downwind plume transport, mechanical interactions between PM and gaseous species and the formation of hybrid PM with altered physicochemical characteristics were observed. Agglomeration and scavenging of volcanic aerosols by the larger fibrous moss fragments were identified as the primary interaction processes and resulted in an increase in the diameter of some particles relative to those in end-member emissions and the removal of the smaller PM size fraction. PM scavenging efficiency did, however, vary between different volatile trace elements. Whilst scavenging and agglomeration are well constrained processes in volcanic plumes; in this compound volcanic-wildfire event they were unique in occurring between emissions from two different sources. These processes thus potentially provide an additional deposition pathway for volcanic aerosols during compound volcanic-wildfire events and may have implications for the transport and exposure risk to certain volcanic heavy metals. Compound volcanic wildfire events therefore present a unique air pollution hazard that influences the issuing of health advice, including emphasising the importance of using respiratory protection to minimize acute exposure to dangerous pollutants (McDonald et al., 2020, Stewart et al., 2021, National Collaborating Centre for Environmental Health (NCCEH), 2025).

In this study, we focus only on the mechanical interactions between volcanic and wildfire PM. However, it is also possible and likely that mixing between volcanic and wildfire emissions may result in chemical reactions between volcanic and wildfire species. For example, the combustion of organic material during wildfires results in the emission of trace, greenhouse, and chemically reactive gases such as CO_2, CO (during incomplete combustion), CH_4, SO_2, NH_3, VOCs, and NO_X species which could have implications for reactive gas phase chemistry if they mix with volcanic gases such as SO_2, HCl, and HF. Identification of these chemical reactions and their implications for atmospheric chemistry remain the exciting remit of future studies. Future work may also consider the toxicological implications of hybrid PM formation in compound events, whether via mechanical interactions, or still unknown chemical reactions. Altered physiochemical characteristics may have implications for the respiratory penetration depth and/or PM toxicity relative to end-member emissions (Tomašek et al., 2016). Constraining the toxicological implications is therefore crucial to correctly inform future health advice. Finally, we emphasise that this work is timely, given that current planetary warming means the severity and frequency of wildfire events, including those ignited by volcanic eruptions, are likely to increase globally over the coming decades.

CRediT authorship contribution statement

Laura Wainman: Writing – review & editing, Writing – original draft, Visualization, Project administration, Methodology, Investigation, Funding acquisition, Formal analysis, Data curation, Conceptualization. **Evgenia Ilyinskaya:** Writing – review & editing, Writing – original draft, Supervision, Project administration, Methodology, Investigation, Funding acquisition, Formal analysis, Data curation, Conceptualization. **Melissa Anne Pfeffer:** Writing – review & editing, Supervision, Resources, Project administration, Methodology, Conceptualization. **Penny E. Wieser:** Writing – review & editing, Visualization, Validation, Supervision, Methodology, Investigation, Formal analysis, Data curation. **David Damby:** Writing – review & editing, Visualization, Methodology, Formal analysis, Data curation. **James B. McQuaid:** Writing – review & editing, Resources, Methodology, Formal analysis, Data curation. **Celine Mandon:** Writing – review & editing, Resources, Investigation, Data curation. **Enikö Bali:** Writing – review & editing, Validation, Resources, Methodology, Investigation, Formal analysis. **Josefa Sepulveda-Araya:** Writing – review & editing, Methodology, Investigation. **Richard Walshaw:** Writing – review & editing, Validation, Software, Resources, Methodology, Investigation, Formal analysis, Data curation. **Caleb Hall:** Software, Resources, Methodology, Formal analysis. **Stuart Micklethwaite:** Writing – review & editing, Software, Resources, Methodology, Formal analysis. **Zabeada Aslam:** Software, Resources, Methodology, Formal analysis. **Samantha J. Hammond:** Writing – review & editing, Software, Resources, Methodology, Formal analysis. **Barbara Kunz:** Writing – review & editing, Software, Resources, Methodology, Formal analysis. **Frances Jenner:** Writing – review & editing, Software, Resources, Methodology, Formal analysis. **Andri Stefánsson:** Resources, Project administration. **Sæmundur A. Halldórsson:** Writing – review & editing, Resources, Project administration. **Jóhann Gunnarsson Robin:** Resources, Project administration. **Alessandro Aiuppa:** Writing – review & editing, Resources, Methodology. **Tamsin A. Mather:** Writing – review & editing, Resources, Project administration.

Declaration of competing interest

The authors declare no competing interests.

Acknowledgements

Laura Wainman acknowledges that this work was supported by the Leeds–York–Hull Natural Environment Research Council (NERC) Doctoral Training Partnership (DTP) Panorama (grant no. NE/S007458/1) and the Icelandic Meteorological Office CASE Partnership. Evgenia Ilyinskaya also acknowledges support from Centre for Observation and Modelling of Earthquakes, Volcanoes and Tectonics (COMET+) and NERC Urgency Grant NE/Z000262/1 "Chemistry of emissions at lava-urban interfaces". Analysis costs were also partially covered by the Icelandic Research Fund (RANNÍS): Magma dynamics on the Reykjanes Peninsula (MaDre) - Integrated geochemical and geophysical investigation of the (on-going) 2021 Fagradalsfjall eruption (grant nr: 228933-053). Penny Wieser acknowledges support from a Sloan Research Fellowship. Alessandro Aiuppa acknowledges funding from the RETURN Extended Partnership funded by the European Union Next-GenerationEU (National Recovery and Resilience Plan – NRRP, Mission). Josefa Sepúlveda-Araya thanks the National Agency for Research and Development (ANID) for the support with the Scholarship

program, Beca de Doctorado en el Extranjero 72210412. We also thank Claire Horwell for kindly lending equipment to support our field campaigns, and the pilots at Svarmi. We thank the Icelandic Meteorological Office and the University of Iceland for their field campaign support and Sandra Piazolo for very helpful discussions on conducting the SEM and TEM analysis. SEM and TEM analysis was carried out at the Leeds Electron Microscopy and Spectroscopy Centre (LEMAS) at the University of Leeds. The authors thank Peter Kelly for providing an internal USGS review and also thank the two reviewers and handling editor for their thorough review and suggestions which have greatly improved the quality of the manuscript. Any use of trade, firm, or product names is for descriptive purposes only and does not imply endorsement by the U.S. Government.

Appendix A. Supplementary data

Supplementary data to this article can be found online at https://doi.org/10.1016/j.scitotenv.2026.181622.

Data availability

The authors declare that all data supporting the findings of this study are available within the paper and in Supplementary Material and Data Sheet. This data is also stored on the CEDA archive.

References

Adachi, K., Dibb, J.E., Scheuer, E., Katich, J.M., Schwarz, J.P., Perring, A.E., Mediavilla, B., Guo, H., Campuzano-Jost, P., Jimenez, J.L., Crawford, J., Soja, A.J., Oshima, N., Mizuo Kajino, Takeshi Kinase, Kleinman, L., Sedlacek, A.J., Yokelson, R. J., Buseck, P.R., 2022. Fine ash-bearing particles as a major aerosol component in biomass burning smoke. J. Geophys. Res. Atmos. 127 (2). https://doi.org/10.1029/2021jd035657.

Aiuppa, A., 2005. Chemical mapping of a fumarolic field: La Fossa crater, Vulcano Island (Aeolian Islands, Italy). Geophys. Res. Lett. 32 (13). https://doi.org/10.1029/2005gl023207.

Aiuppa, A., 2009. Degassing of halogens from basaltic volcanism: insights from volcanic gas observations. Chem. Geol. 263 (1–4), 99–109. https://doi.org/10.1016/j.chemgeo.2008.08.022.

Almannavarnir, 2023. Óvissustigi Almannavarna vegna jarðskjálftahrinu á Reykjanesskaga aflýst. [online] Almannavarnir. Available at https://www.almannavarnir.is/frettir/ovissustigi-almannavarna-vegna-jardskjalftahrinu-a-reykjanesskaga-aflyst/. (Accessed 5 December 2025).

Ammann, M., Burtscher, H., 1993. Aerosol dynamics and light-scattering properties of a volcanic plume. J. Geophys. Res. Solid Earth 98 (B11), 19705–19711. https://doi.org/10.1029/93jb02003.

Arndt, J., Calabrese, S., D'Alessandro, W., Planer-Friedrich, B., 2017. Using mosses as biomonitors to study trace element emissions and their distribution in six different volcanic areas. J. Volcanol. Geotherm. Res. 343, 220–232. https://doi.org/10.1016/j.jvolgeores.2017.07.004.

Balcaen, L., Bolea-Fernandez, E., Resano, M., Vanhaecke, F., 2015. Inductively coupled plasma – tandem mass spectrometry (ICP-MS/MS): A powerful and universal tool for the interference-free determination of (ultra)trace elements – A tutorial review. Anal. Chim. Acta 894, 7–19. https://doi.org/10.1016/j.aca.2015.08.053.

Brown, R.J., Bonadonna, C., Durant, A.J., 2012. A review of volcanic ash aggregation. Physics and Chemistry of the Earth, Parts A/B/C 45-46, 65–78. https://doi.org/10.1016/j.pce.2011.11.001.

Butwin, M.K., Pfeffer, M.A., von Löwis, S., Støren, E.W.N., Bali, E., Thorsteinsson, T., 2020. Properties of dust source material and volcanic ash in Iceland. Sedimentology. https://doi.org/10.1111/sed.12734.

Caracciolo, A., Marshall, E.W., Mutch, E.J.F., Bali, E., Halldórsson, S.A., Matthews, S., Sigmarsson, Olgeir, Maclennan, J., Merrill, H., Gisladóttir, Bryndís Ýr, Johnson, S., Kahl, M., Guðfinnsson, G.H., Robin, J.G., Rúnarsdóttir, R.H., 2025. Mush disaggregation and dike propagation timescales at active volcanoes – evidence from the 2022-2023 Fagradalsfjall eruptions. J. Petrol. https://doi.org/10.1093/petrology/egaf054.

Chen, W., Ge, P., Lu, Z., Liu, X., Cao, M., Yan, Z., Chen, M., 2024. Acute exposure to seasonal PM2.5 induces toxicological responses in A549 cells cultured at the air-liquid interface mediated by oxidative stress and endoplasmic reticulum stress. Environ. Res. 118283. https://doi.org/10.1016/j.envres.2024.118283 [online] 248,.

Chu, D., Grasby, S.E., Song, H., Corso, J.D., Wang, Y., Mather, T.A., Wu, Y., Song, H., Shu, W., Tong, J., Wignall, P.B., 2020. Ecological disturbance in tropical peatlands prior to marine Permian-Triassic mass extinction. Geology 48 (3), 288–292. https://doi.org/10.1130/g46631.1.

Cox, D., Watt, S.F.L., Jenner, F.E., Hastie, A.R., Hammond, S.J., 2019. Chalcophile element processing beneath a continental arc stratovolcano. Earth and Planetary Science Letters, [online] 522, 1–11. https://doi.org/10.1016/j.epsl.2019.06.017.

Crilley, L.R., Shaw, M., Pound, R., Kramer, L.J., Price, R., Young, S., Lewis, A.C., Pope, F. D., 2018. Evaluation of a low-cost optical particle counter (Alphasense OPC-N2) for ambient air monitoring. Atmos. Meas. Tech. 11 (2), 709–720. https://doi.org/10.5194/amt-11-709-2018.

Delmelle, P., 2003. Environmental impacts of tropospheric volcanic gas plumes. Geol. Soc. Lond. Spec. Publ. 213 (1), 381–399. https://doi.org/10.1144/gsl.sp.2003.213.01.23.

Faherty, T., Raymond, J.E., McFiggans, G., Pope, F.D., 2025. Acute particulate matter exposure diminishes executive cognitive functioning after four hours regardless of inhalation pathway. Nat. Commun. 16 (1). https://doi.org/10.1038/s41467-025-56508-3.

Fink, J., Ajibade, I., 2022. Future impacts of climate-induced compound disasters on volcano hazard assessment. Bull. Volcanol. 84 (5). https://doi.org/10.1007/s00445-022-01542-y.

Grusak, M.A., Broadley, M.R., White, P.J., 2016. Plant macro- and micronutrient minerals. eLS, [online], pp. 1–6. https://doi.org/10.1002/9780470015902.a0001306.pub2.

Halldórsson, S.A., Marshall, E.W., Caracciolo, A., Matthews, S., Bali, E., Rasmussen, M.B., Ranta, E., Robin, J.G., Guðfinnsson, G.H., Sigmarsson, O., Maclennan, J., Jackson, M.G., Whitehouse, M.J., Jeon, H., van der Meer, Q.H.A., Mibei, G.K., Kalliokoski, M.H., Repczynska, M.M., Rúnarsdóttir, R.H., Sigurðsson, G., 2022. Rapid shifting of a deep magmatic source at Fagradalsfjall volcano, Iceland. Nature, [online] 609 (7927), 529–534. https://doi.org/10.1038/s41586-022-04981-x.

Holder, A.L., Rao, V., Kovalcik, K., Virtaranta, L., 2023. Particulate Pb emission factors from wildland fires in the United States. Atmospheric Environment: X 20, 100229. https://doi.org/10.1016/j.aeaoa.2023.100229.

Hovington, P., Drouin, D., Gauvin, R., 2006. CASINO: A new Monte Carlo code in C language for electron beam interaction -part I: description of the program. Scanning 19 (1), 1–14. https://doi.org/10.1002/sca.4950190101.

Iacono, F., Bisson, M., Spinetti, C., Kwasnitschka, T., 2025. Wildfires induced by volcanic activity at Stromboli Island during the 2019 summer through satellite and drone data. Remote Sensing in Earth Systems Sciences. https://doi.org/10.1007/s41976-025-00215-6.

Icelandic Environment Agency, 2025. Loftgæði á Íslandi. [online] Xn–loftgi-tua4f.is. Available at https://xn–loftgi-tua4f.is/?zoomLevel=7&lat=64.894972&lng=-18.675028. (Accessed 22 October 2025).

Icelandic Institute of Natural History, 2023. Mosabruni á gosstöðvunum við Litla-Hrút. [online] Náttúrufræðistofnun Íslands. Available at https://www.natt.is/is/frettir/2023/07/mosabruni-gosstodvunum-vid-litla-hrut. (Accessed 5 December 2025).

Icelandic Met Office, 2018. Climate Report | Climate of Iceland. [online] Icelandic Meteorological Office. Available at https://en.vedur.is/climatology/iceland/climate-report.

Ilyinskaya, E., Mason, E., Wieser, P.E., Holland, L., Liu, E.J., Mather, T.A., Edmonds, M., Whitty, R.C., Elias, T., Nadeau, P.A., Schneider, D., 2021. Rapid metal pollutant deposition from the volcanic plume of Kīlauea, Hawai'i. Commun. Earth Environ. 2 (1), 78.

Kajino, M., Ueda, H., Satsumabayashi, H., An, J., 2004. Impacts of the eruption of Miyakejima volcano on air quality over far East Asia. J. Geophys. Res. Atmos. 109 (D21). https://doi.org/10.1029/2004jd004762.

Liu, E.J., Aiuppa, A., Alan, A., Arellano, S., Bitetto, M., Bobrowski, N., Carn, S., Clarke, R., Corrales, E., de Moor, J.M., Diaz, J.A., Edmonds, M., Fischer, T.P., Freer, J., Fricke, G.M., Galle, B., Gerdes, G., Giudice, G., Gutmann, A., Hayer, C., 2020. Aerial strategies advance volcanic gas measurements at inaccessible, strongly degassing volcanoes. Science. Advances 6 (44). https://doi.org/10.1126/sciadv.abb9103 p.eabb9103.

Mansoor, S., Farooq, I., Kachroo, M.M., Mahmoud, A.E.D., Fawzy, M., Popescu, S.M., Alyemeni, M.N., Sonne, C., Rinklebe, J., Ahmad, P., 2022. Elevation in wildfire frequencies with respect to the climate change. J. Environ. Manag. 301 (113769), 113769. https://doi.org/10.1016/j.jenvman.2021.113769.

Martin, R.M., Mather, T.A., Pyle, D.M., Power, M., Allen, A.M., Alessandro Aiuppa, Horwell, C.J., Ward, 2008. Composition-resolved size distributions of volcanic aerosols in the Mt. Etna plumes. J. Geophys. Res. Atmos. 113 (D17). https://doi.org/10.1029/2007jd009648.

Mason, E., Wieser, P.E., Liu, E.J., Edmonds, M., Ilyinskaya, E., Whitty, R.C.W., Mather, T. A., Elias, T., Nadeau, P.A., Wilkes, T.C., McGonigle, A.J.S., Pering, T.D., Mims, F.M., Kern, C., Schneider, D.J., Oppenheimer, C., 2021. Volatile metal emissions from volcanic degassing and lava–seawater interactions at Kīlauea volcano, Hawai'i. Communications Earth & Environment, [online] 2 (1), 1–16. https://doi.org/10.1038/s43247-021-00145-3.

Mather, T.A., Pyle, D.M., Oppenheimer, C., 2003. Tropospheric volcanic aerosol. In: Volcanism and the Earth's Atmosphere, pp. 189–212. https://doi.org/10.1029/139gm12 online.

Mather, T.A., Witt, M.L.I., Pyle, D.M., Quayle, B.M., Aiuppa, A., Bagnato, E., Martin, R.S., Sims, K.W.W., Edmonds, M., Sutton, A.J., Ilyinskaya, E., 2012. Halogens and trace metal emissions from the ongoing 2008 summit eruption of Kīlauea volcano, Hawai'i. Geochim. Cosmochim. Acta 83, 292–323. https://doi.org/10.1016/j.gca.2011.11.029.

McDonald, F., Horwell, C.J., Wecker, R., Dominelli, L., Loh, M., Kamanyire, R., Ugarte, C., 2020. Facemask use for community protection from air pollution disasters: An ethical overview and framework to guide agency decision making. International Journal of Disaster Risk Reduction 43, 101376. https://doi.org/10.1016/j.ijdrr.2019.101376.

Meredith, E.S., Jenkins, S.F., Hayes, J.L., Deligne, N.I., Lallemant, D., Patrick, M., Neal, C., 2022. Damage assessment for the 2018 lower east rift zone lava flows of Kīlauea volcano, Hawai'i. Bull. Volcanol. 84 (7). https://doi.org/10.1007/s00445-022-01568-2.

National Collaborating Centre for Environmental Health (NCCEH), 2025. Rapid review: Evaluating the effectiveness of masks and respirators against wildfire smoke. [online] National Collaborating Centre for Environmental Health | NCCEH - CCSNE. Available at https://ncceh.ca/resources/evidence-reviews/rapid-review-evaluating-effectiveness-masks-and-respirators-against.

Nriagu, J.O., 1989. A global assessment of natural sources of atmospheric trace metals. Nature 338 (6210), 47–49. https://doi.org/10.1038/338047a0.

Opravilová, V., Zahrádková, S., 2003. Some information on testate amoebae of Iceland. Limnologica 33 (2), 131–137. https://doi.org/10.1016/s0075-9511(03)80042-7.

Perron, M.M.G., Meyerink, S., Corkill, M., Strzelec, M., Proemse, B.C., Gault-Ringold, M., Sanz Rodriguez, E., Chase, Z., Bowie, A.R., 2022. Trace elements and nutrients in wildfire plumes to the southeast of Australia. Atmos. Res. 270, 106084. https://doi.org/10.1016/j.atmosres.2022.106084.

Pokhrel, R.P., Gordon, J., Fiddler, M.N., Bililign, S., 2020. Impact of combustion conditions on physical and morphological properties of biomass burning aerosol. Aerosol Sci. Technol. 55 (1), 80–91. https://doi.org/10.1080/02786826.2020.1822512.

Reid, C.E., Brauer, M., Johnston, F.H., Jerrett, M., Balmes, J.R., Elliott, C.T., 2016. Critical review of health impacts of wildfire smoke exposure. Environ. Health Perspect. 124 (9), 1334–1343. https://doi.org/10.1289/ehp.1409277 online.

Robinson, H., 1971. Scanning electron microscope studies on moss leaves and peristomes. Bryologist 473–483.

Rose, W.I., 1977. Scavenging of volcanic aerosol by ash: atmospheric and volcanologic implications. Geology 5 (10), 621. https://doi.org/10.1130/0091-7613(1977)5%3C621:sovaba%3E2.0.co;2.

Schiffmann, J., Walter, T.R., Sobolewski, L., Heinken, Thilo, 2025. Volcanic eruptions and Moss heath wildfires on Iceland's Reykjanes peninsula: satellite and field perspectives on disturbance and recovery. GeoHazards, [online] 6 (4), 70. https://doi.org/10.3390/geohazards6040070.

Schmidt, A., Leadbetter, S., Theys, N., Carboni, E., Witham, C.S., Stevenson, J.A., Birch, C.E., Thordarson, T., Turnock, S., Barsotti, S., Delaney, L., Feng, W., Grainger, R.G., Hort, M.C., Höskuldsson, Á., Ialongo, I., Ilyinskaya, E., Jóhannsson, T., Kenny, P., Mather, T.A., 2015. Satellite detection, long-range transport, and air quality impacts of volcanic sulfur dioxide from the 2014–2015 flood lava eruption at Bárðarbunga (Iceland). J. Geophys. Res. Atmos. 120 (18), 9739–9757. https://doi.org/10.1002/2015jd023638.

Selimovic, V., Yokelson, R.J., McMeeking, G.R., Coefield, S., 2019. In situ measurements of trace gases, PM, and aerosol optical properties during the 2017 NW US wildfire smoke event. Atmos. Chem. Phys. 19 (6), 3905–3926. https://doi.org/10.5194/acp-19-3905-2019.

Shatto, C., Kiene, M., Hofmann, P., Walentowitz, A., Wilkens, V., Heuser, T., Weiser, F., 2024. Assessing the recovery of *Pinus canariensis* stands after wildfires and volcanic eruption on La Palma, Canary Islands. For. Ecol. Manag. 572, 122317. https://doi.org/10.1016/j.foreco.2024.122317 online.

Sigtryggsdóttir, F.G., Hrafnsdóttir, H., Steingrímsson, J.H., Guðmundsson, A., 2025. Experience in diverting and containing lava flow by barriers constructed from in situ material during the 2021 Geldingardalir volcanic eruption. Bull. Volcanol. 87 (4). https://doi.org/10.1007/s00445-025-01806-3.

Stewart, C., Damby, D.E., Horwell, C.J., Elias, T., Ilyinskaya, E., Tomašek, I., Longo, B.M., Schmidt, A., Carlsen, H.K., Mason, E., Baxter, P.J., Cronin, S., Witham, C., 2021. Volcanic air pollution and human health: recent advances and future directions. Bull. Volcanol. 84 (1). https://doi.org/10.1007/s00445-021-01513-9 online.

Tang, H., Meng, G., Xiang, J., Mahmood, A., Xiang, G., SanaUllah, Liu, Y., Huang, G., 2022. Toxic effects of antimony in plants: reasons and remediation possibilities—a review and future prospects. Front. Plant Sci. 13, 1011945. https://doi.org/10.3389/fpls.2022.1011945 online.

Tomašek, I., Horwell, C.J., Damby, D.E., Barosova, H., Geers, C., Alke Petri-Fink, Rothen-Rutishauser, B., Clift, M., 2016. Combined exposure of diesel exhaust particles and respirable Soufrière Hills volcanic ash causes a (pro-)inflammatory response in an in vitro multicellular epithelial tissue barrier model. Part. Fibre Toxicol. 13 (1). https://doi.org/10.1186/s12989-016-0178-9.

Turchi, A., Di Traglia, F., Luti, T., Olori, D., Zetti, I., Fanti, R., 2020. Environmental aftermath of the 2019 Stromboli eruption. Remote Sens. 12 (6), 994. https://doi.org/10.3390/rs12060994.

Varela, Z., Boquete, M.T., Fernández, J.Á., Martínez-Abaigar, J., Núñez-Olivera, Encarnación, Aboal, J.R., 2023. Mythbusters: unravelling the pollutant uptake processes in mosses for air quality biomonitoring. Ecol. Indic. 148, 110095. https://doi.org/10.1016/j.ecolind.2023.110095.

Vasilatou, K., Wälchli, C., Koust, S., Horender, S., Iida, K., Sakurai, H., Schneider, F., Spielvogel, J., Wu, T.Y., Auderset, K., 2021. Calibration of optical particle size spectrometers against a primary standard: counting efficiency profile of the TSI model 3330 OPS and Grimm 11-D monitor in the particle size range from 300 nm to 10 μm. Journal of Aerosol Science, [online] 157, 105818. https://doi.org/10.1016/j.jaerosci.2021.105818.

Veðurstofa íslands, 2023. Veðurfarsyfirlit - Keflavíkurflugvöllur Júlí 2023 [online] Available at https://www.vedur.is/vedur/vedurfar/daglegt/keflavik/.

Voiland, A., 2023. Landsat Image Gallery - Lava and Smoke Blanket Fagradalsfjall. [online] Nasa.gov. Available at: https://landsat.visibleearth.nasa.gov/view.php?id=151653. (Accessed 11 September 2025).

Wainman, L., 2024. Using drones to sample volcanic plumes. Nature Reviews Earth & Environment, [online] 5 (7), 484. https://doi.org/10.1038/s43017-024-00570-w.

Wainman, L., Ilyinskaya, E., Pfeffer, M., Mandon, C., Bali, E., Edwards, B.A., Kleine-Marshall, B.I., Gudjonsdottir, S.R., Cotterill, A., Scott, S.W., Wieser, P., Stefánsson, A., Nicholson, E.J., Sepulveda-Araya, J., Hammond, S.J., Kunz, B.E., Jenner, F., Gunnarsson, J.R., Aiuppa, A., Burton, M., 2024a. Trace Element Emissions Vary With Lava Flow Age and Thermal Evolution During the Fagradalsfjall 2021–2023 Eruptions, Iceland. Geochem. Geophys. Geosyst. 25 (12). https://doi.org/10.1029/2024gc011822.

Pre-print Wainman, L., Ilyinskaya, E., Pfeffer, M., Mandon, C., Bali, E., Edwards, B.A., Kleine-Marshall, B.I., Gudjonsdottir, S.R., Cotterill, A., Wieser, P., Stefánsson, A., Nicholson, E.J., Hammond, S.J., Kunz, B.E., Jenner, F., Gunnarsson, J.R., Aiuppa, A., Burton, M., 2024b. Heterogeneous trace element deposition from an effusive volcanic plume. In: Review. https://www.researchsquare.com/article/rs-6665526/v1.

Wardman, J., Sword-Daniels, V., Stewart, C., Wilson, T., 2012. Impact assessment of the May 2010 eruption of Pacaya volcano, Guatemala.

Wesely, M., Hicks, B., 2000. A review of the current status of knowledge on dry deposition. Atmos. Environ.Atmospheric Environment 34 (12–14), 2261–2282. https://doi.org/10.1016/s1352-2310(99)00467-7.

Whitty, R., Ilyinskaya, E., Pfeffer, M.A., Thrastarson, R.H., Sæmundsson, G.G., 2025. Fine-scale fluctuations of PM 1 , PM 2.5 , PM 10 and SO 2 concentrations caused by a prolonged volcanic eruption (Fagradalsfjall 2021, Iceland). [online] EGUSphere. https://doi.org/10.5194/egusphere-2025-937.

Wilson, A.L., Cui, W., Hu, Y., Chiapasco, M., Rein, G., Porter, A.E., Fowler, G., Stettler, M. E.J., 2025. Particles emitted from smouldering peat: size-resolved composition and emission factors. Environ. Sci. Atmos. https://doi.org/10.1039/d4ea00124a online.

Witham, C.S., Oppenheimer, C., Horwell, C.J., 2005. Volcanic ash-leachates: a review and recommendations for sampling methods. J. Volcanol. Geotherm. Res. 141 (3–4), 299–326. https://doi.org/10.1016/j.jvolgeores.2004.11.010.

Yong Quah, J., Hayes, J.L., Fitzgerald, R.H., Lerner, G.A., Jenkins, S.F., Wilson, T.M., Scheele, F., Lukovic, B., Fleischmann, C., 2023. Fire from volcanic activity: quantifying the threat from an understudied hazard. Fire Saf. J. 141, 103935. https://doi.org/10.1016/j.firesaf.2023.103935 online.